

1 **Humans strategically shift decision bias by flexibly**
2 **adjusting sensory evidence accumulation**

3

4 Niels A. Kloosterman^{*1,2}, Jan Willem de Gee³, Markus Werkle-Bergner², Ulman
5 Lindenberger^{1,2}, Douglas D. Garrett^{1,2+}, Johannes Jacobus Fahrenfort^{4,5+}

6

7 ¹ Max Planck UCL Centre for Computational Psychiatry and Ageing Research, Max Planck Institute
8 for Human Development, Lentzeallee 94, 14195 Berlin, Germany

9 ² Center for Lifespan Psychology, Max Planck Institute for Human Development, Lentzeallee 94,
10 14195 Berlin, Germany

11 ³ Department of Neurophysiology and Pathophysiology, University Medical Center Hamburg-
12 Eppendorf, Germany;

13 ⁴ Department of Psychology, University of Amsterdam, The Netherlands;

14 ⁵ Department of Experimental and Applied Psychology, Vrije Universiteit, van der Boechorststraat 1,
15 1081 BT Amsterdam, The Netherlands

16 ⁺Shared senior author

17 *Correspondence: kloosterman@mpib-berlin.mpg.de

18

19 **Corresponding author information**

20 Niels A. Kloosterman, Ph.D.

21 Max Planck UCL Centre for Computational Psychiatry and Ageing Research,
22 Lentzeallee 94, 14195, Berlin, Germany

23 Phone: +49 30 82406 424

24 E-mail: kloosterman@mpib-berlin.mpg.de

25 **Abstract**

26 Decision bias is traditionally conceptualized as an internal reference against which
27 sensory evidence is compared. Instead, we show that individuals implement decision
28 bias by shifting the rate of sensory evidence accumulation towards a decision bound.
29 Participants performed a target detection task while we recorded EEG. We
30 experimentally manipulated participants' decision criterion for reporting targets using
31 different stimulus-response reward contingencies, inducing either a liberal or a
32 conservative bias. Drift diffusion modeling revealed that a liberal strategy biased
33 sensory evidence accumulation towards target-present choices. Moreover, a liberal
34 bias resulted in stronger midfrontal pre-stimulus 2–6 Hz (theta) power and
35 suppression of pre-stimulus 8–12 Hz (alpha) power in posterior cortex. The alpha
36 suppression in turn mediated the output activity of visual cortex, as expressed in
37 59–100 Hz (gamma) power. These findings show that observers can intentionally
38 control cortical excitability to strategically bias evidence accumulation towards the
39 decision bound that maximizes their reward.

40

41 **Introduction**

42 Perceptual decisions arise not only from the evaluation of sensory evidence, but are
43 often biased towards one or another choice alternative by environmental factors,
44 perhaps as a result of task instructions and/or stimulus-response reward
45 contingencies (White & Poldrack, 2014). The ability to willfully control decision bias
46 could potentially enable the behavioral flexibility required to survive in an ever-
47 changing and uncertain environment. But despite its important role in decision
48 making, the neural mechanisms underlying decision bias are not fully understood.

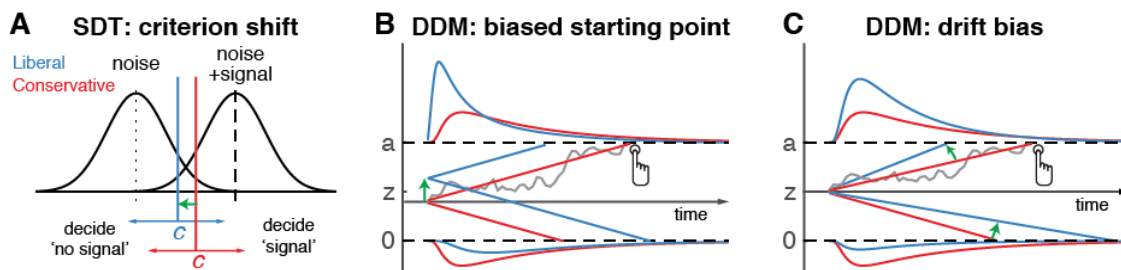
49 The traditional account of decision bias comes from signal detection theory
50 (SDT) (Green & Swets, 1966). In SDT, decision bias is quantified by estimating the

51 relative position of a decision point or 'criterion' in between sensory evidence
52 distributions for noise and signal (see Figure 1A). In this framework, a more liberal
53 decision bias arises by moving the criterion closer towards the noise distribution (see
54 green arrow in Figure 1A). Although SDT has been very successful at quantifying
55 decision bias, how exactly bias affects decision making and how it is reflected in
56 neural activity remains unknown.

57 One reason for this lack of insight may be that SDT does not have a temporal
58 component to track how decisions are reached over time (Fetsch, Kiani, & Shadlen,
59 2014). As an alternative to SDT, the drift diffusion model (DDM) conceptualizes
60 perceptual decision making as the accumulation of noisy sensory evidence over time
61 into an internal decision variable (Bogacz, Brown, Moehlis, Holmes, & Cohen, 2006;
62 Gold & Shadlen, 2007; Ratcliff & McKoon, 2008). A decision in this model is made
63 when the decision variable crosses one of two decision bounds corresponding to the
64 choice alternatives. After one of the bounds is reached, the corresponding decision
65 can subsequently either be actively reported, for example by means of a button
66 press indicating a detected signal, or it could remain without behavioral report when
67 no signal is detected (Ratcliff, Huang-Pollock, & McKoon, 2016). Within this
68 framework, a strategic decision bias imposed by the environment can be modelled in
69 two different ways: either by moving the starting point of evidence accumulation
70 closer to one of the boundaries (see green arrow in Figure 1B), or by biasing the rate
71 of the evidence accumulation process itself towards one of the boundaries (see
72 green arrow in Figure 1C). In both the SDT and DDM frameworks, decision bias
73 shifts have little effect on the sensitivity of the observer when distinguishing signal
74 from noise; they predominantly affect the relative response ratios (and in the case of
75 DDM the speed with which one or the other decision bound is reached). There has

76 been some evidence to suggest that decision bias induced by shifting the criterion is
77 best characterized by a drift bias in the DDM (Urai, de Gee, & Donner, 2018; White &
78 Poldrack, 2014). However, the drift bias parameter has as yet not been related to a
79 well-described neural mechanism.

80



81

82 **Figure 1 | Theoretical accounts of decision bias.** **A.** Signal-detection-theoretic account of decision
83 bias. Signal and noise+signal distributions are plotted as a function of the strength of internal sensory
84 evidence. The decision point (or criterion) that determines whether to decide signal presence or
85 absence is plotted as a vertical criterion line c , reflecting the degree of decision bias. c can be shifted
86 left- or rightwards to denote a more liberal or conservative bias, respectively (green arrow indicates a
87 shift towards more liberal). **B, C:** Drift diffusion model (DDM) account of decision bias, in which
88 decisions are modelled in terms of a set of parameters that describe a dynamic process of sensory
89 evidence accumulation towards one of two decision bounds. When sensory input is presented,
90 evidence starts to accumulate (drift) over time after initialization at the starting point z . A decision is
91 made when the accumulated evidence either crosses decision boundary a (signal presence) or
92 decision boundary 0 (no signal). After a boundary is reached, the corresponding decision can be
93 either actively reported by a button press (e.g. for signal-present decisions), or remain implicit, without
94 a response (for signal-absent decisions). The DDM can capture decision bias through a shift of the
95 starting point of the evidence accumulation process (panel B) or through a shift in bias in the rate of
96 evidence accumulation towards the different choices (panel C). These mechanisms are dissociable
97 through their differential effect on the shape of the reaction time (RT) distributions, as indicated by the
98 curves above and below the graphs for target-present and target-absent decisions, respectively.
99 Panels B. and C. are modified and reproduced with permission from Urai, de Gee, & Donner (2018)
100 (Figure 1, published under a CC BY 4.0 license).

101

102 Regarding the neural underpinnings of decision bias, there have been a
103 number of reports about a correlational relationship between cortical population
104 activity measured with EEG and decision bias. For example, spontaneous trial-to-
105 trial variations in pre-stimulus oscillatory activity in the 8–12 Hz (alpha) band have
106 been shown to correlate with decision bias and confidence (Iemi, Chaumon, Crouzet,
107 & Busch, 2017; Limbach & Corballis, 2016; Samaha, Iemi, & Postle, 2017). Alpha
108 oscillations, in turn, have been proposed to be involved in the gating of task-relevant
109 sensory information (Jensen & Mazaheri, 2010) possibly encoded in high-frequency
110 (gamma) oscillations in visual cortex (Ni et al., 2016; Popov, Kastner, & Jensen,
111 2017). Although these reports suggest links between pre-stimulus alpha
112 suppression, sensory information gating and decision bias, they do not uncover
113 whether pre-stimulus alpha plays an instrumental role in decision bias and how
114 exactly this might be achieved. Specifically, it is unknown whether an experimentally
115 induced shift in decision bias is implemented in the brain by willfully adjusting pre-
116 stimulus alpha in sensory areas.

117 Here, we explicitly investigate these potential mechanisms by employing a
118 task paradigm in which shifts in decision bias were experimentally induced within
119 participants through (a) instruction and (b) asymmetries in stimulus-response reward
120 contingencies during a visual target detection task. By applying drift diffusion
121 modeling to the participants' choice behavior, we show that the effect of strategically
122 adjusting decision bias is best captured by the drift bias parameter, which is thought
123 to reflect the rate of sensory evidence accumulation towards one of the two decision
124 bounds. To substantiate a neural mechanism for this effect, we demonstrate that this
125 bias shift is accompanied by changes in pre-stimulus midfrontal 2–6 Hz (theta)

126 power, as well as changes in sensory alpha suppression. Pre-stimulus alpha
127 suppression in turn mediates the output post-stimulus activity of visual cortex, as
128 reflected in gamma power modulation. Critically, we show that gamma activity
129 accurately predicts the strength of evidence accumulation bias within participants,
130 providing a direct link between the proposed mechanism and decision bias.
131 Together, these findings identify the neural mechanism by which intentional control
132 of cortical excitability is applied to strategically bias perceptual decisions in order to
133 maximize reward in a given ecological context.

134

135 **Results**

136 **Manipulation of decision bias affects sensory evidence accumulation**

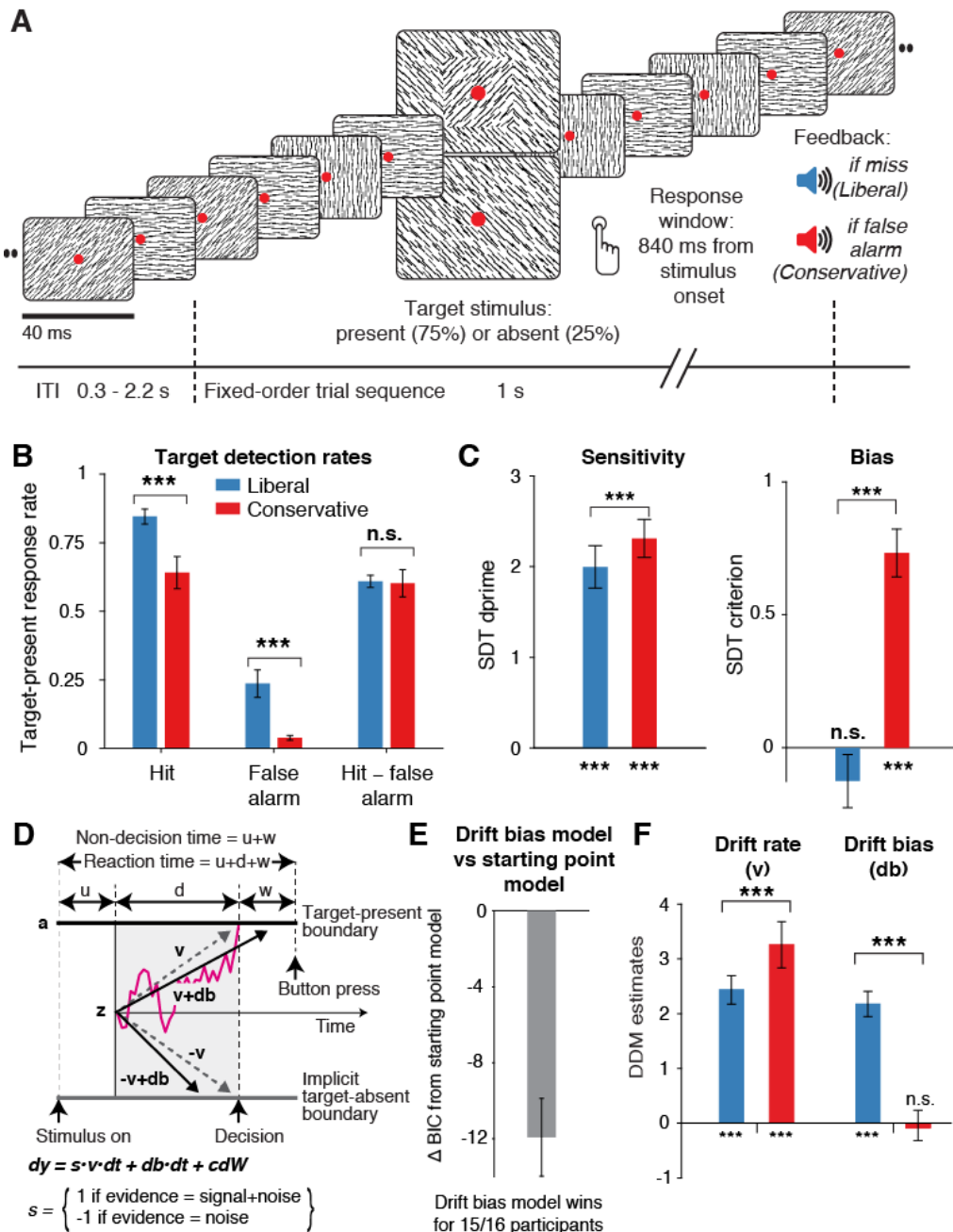
137 In three EEG recording sessions, human participants (N = 16) viewed a continuous
138 stream of horizontal, vertical and diagonal line textures alternating at a rate of 25
139 textures/second. The participants' task was to detect an orientation-defined square
140 presented in the center of the screen and report it via a button press (Figure 2A).
141 Trials consisted of a fixed-order sequence of textures embedded in the continuous
142 stream (total sequence duration 1 second). A square appeared in the fifth texture of
143 a trial in 75% of the presentations (target trials), while in 25% a homogenous
144 diagonal texture appeared in the fifth position (nontarget trials). Although the onset of
145 a trial within the continuous stream of textures was not explicitly cued, the similar
146 distribution of reaction times in target and nontarget trials suggests that participants
147 used the temporal structure of the task even when no target appeared (Figure 2—
148 figure supplement 1A). Consistent and significant EEG power modulations after trial
149 onset (even for nontarget trials) further confirm that subjects registered trial onsets in

150 the absence of an explicit cue, plausibly using the onset of a fixed order texture
151 sequence as an implicit cue (Figure 2—figure supplement 1B).

152 In alternating nine-minute blocks of trials, we actively biased participants'
153 perceptual decisions by instructing them either to report as many targets as possible
154 ("Detect as many targets as possible!"; liberal condition), or to only report high-
155 certainty targets ("Press only if you are really certain!"; conservative condition).
156 Participants were free to respond at any time during a block whenever they detected
157 a target. A trial was considered a target present response when a button press
158 occurred before the fixed-order sequence ended (i.e. within 0.84 s after onset of the
159 fifth texture containing the (non)target, see Figure 2A). We provided auditory
160 feedback and applied monetary penalties following missed targets in the liberal
161 condition and following false alarms in the conservative condition (Figure 2A; see
162 Methods for details). The median number of trials for each SDT category across
163 participants was 1206 hits, 65 false alarms, 186 misses and 355 correct rejections in
164 the liberal condition, and 980 hits, 12 false alarms, 419 misses and 492 correct
165 rejections in the conservative condition.

166 Participants reliably adopted the intended decision bias shift across the two
167 conditions, as shown by both the hit rate and the false alarm rate going down in
168 tandem as a consequence of a more conservative bias (Figure 2B). The difference
169 between hit rate and false alarm rate was not significantly modulated by the
170 experimental bias manipulations ($p = 0.81$, two-sided permutation test, 10,000
171 permutations, see Figure 2B). However, target detection performance computed
172 using standard SDT d' (perceptual sensitivity, reflecting the distance between the
173 noise and signal distributions in Figure 1A)(Green & Swets, 1966) was slightly higher
174 during conservative (liberal: $d' = 2.0$ (s.d. 0.90) versus conservative: $d' = 2.31$ (s.d.

175 0.82), $p = 0.0002$, see Figure 2C, left bars). We quantified decision bias using the
176 standard SDT criterion measure c , in which positive and negative values reflect
177 conservative and liberal biases, respectively (see the blue and red vertical lines in
178 Figure 1A). This uncovered a strong experimentally induced bias shift from the
179 conservative to the liberal condition (liberal: $c = -0.13$ (s.d. 0.4), versus
180 conservative: $c = 0.73$ (s.d. 0.36), $p = 0.0001$, see Figure 2C), as well as a
181 conservative average bias across the two conditions ($c = 0.3$ (s.d. 0.31), $p = 0.0013$).



182

183 **Figure 2 | Strategic decision bias shift towards liberal biases evidence accumulation. A.**
184 Schematic of the visual stimulus and task design. Participants viewed a continuous stream of full-
185 screen diagonally, horizontally and vertically oriented textures at a presentation rate of 40 ms (25 Hz).
186 After random inter-trial intervals, a fixed-order sequence was presented embedded in the stream. The
187 fifth texture in each sequence either consisted of a single diagonal orientation (target absent), or
188 contained an orthogonal orientation-defined square (either 45° or 135° orientation). Participants
189 decided whether they had just seen a target, reporting detected targets by button press. Liberal and

190 conservative conditions were administered in alternating nine-minute blocks by penalizing either
191 misses or false alarms, respectively, using aversive tones and monetary deductions. Depicted square
192 and fixation dot sizes are not to scale. **B.** Average detection rates (hits and false alarms) during both
193 conditions. Miss rate is equal to 1 – hit rate since both are computed on stimulus present trials, and
194 correct-rejection rate is equal to 1 – false alarm rate since both are computed on stimulus absent
195 trials, together yielding the four SDT stimulus-response categories **C.** SDT parameters for sensitivity
196 and criterion. **D.** Schematic and simplified equation of drift diffusion model accounting for reaction
197 time distributions for actively reported target-present and implicit target-absent decisions. Decision
198 bias in this model can be implemented by either shifting the starting point of the evidence
199 accumulation process (Z), or by adding an evidence-independent constant ('drift bias', db) to the drift
200 rate. See text and Figure 1 for details. Notation: dy , change in decision variable y per unit time dt ; $v \cdot dt$,
201 mean drift (multiplied with 1 for signal + noise (target) trials, and -1 for noise-only (nontarget) trials);
202 $db \cdot dt$, drift bias; and cdW , Gaussian white noise (mean = 0, variance = $c2 \cdot dt$). **E.** Difference in
203 Bayesian Information Criterion (BIC) goodness of fit estimates for the drift bias and the starting point
204 models. A lower delta BIC value indicates a better fit, showing superiority of the drift bias model to
205 account for the observed results. **F.** Estimated model parameters for drift rate and drift bias in the drift
206 bias model. Error bars, SEM across 16 participants. *** $p < 0.001$; n.s., not significant. Panel D. is
207 modified and reproduced with permission from (de Gee et al., 2017) (Figure 4A, published under a
208 CC BY 4.0 license).

209 The following source data and figure supplements are available for Figure 2:

210 **Source data 1.** This csv table contains the data for Figure 2 panels B, C, E and F.

211 **Figure supplement 1.** Behavioral and neurophysiological evidence that participants were sensitive to
212 the implicit task structure.

213 **Figure supplement 2.** Signal-detection-theoretic behavioral measures during both conditions
214 correspond closely to drift diffusion modeling parameters.

215 **Figure supplement 3.** Single-participant drift diffusion model fits for the drift bias model for both
216 conditions.

217 Because the SDT framework is static over time, we further investigated how
218 bias affected various components of the dynamic decision process by fitting different
219 variants of the drift diffusion model (DDM) to the behavioral data (Figure 1B, C)
220 (Ratcliff & McKoon, 2008). The DDM postulates that perceptual decisions are
221 reached by accumulating noisy sensory evidence towards one of two decision
222 boundaries representing the choice alternatives. Crossing one of these boundaries
223 can either trigger an explicit behavioral report to indicate the decision (for target-
224 present responses in our experiment), or remain implicit (i.e. without active
225 response, for target-absent decisions in our experiment). The DDM captures the
226 dynamic decision process by estimating parameters reflecting the rate of evidence
227 accumulation (drift rate), the separation between the boundaries, as well as the time
228 needed for stimulus encoding and response execution (non-decision time) (Ratcliff &
229 McKoon, 2008). The DDM is able to estimate these parameters based on the shape
230 of the RT distributions for actively reported (target-present) decisions along with the
231 total number of trials in which no response occurred (i.e. implicit target-absent
232 decisions) (Ratcliff et al., 2016).

233 We fitted two variants of the DDM to distinguish between two possible
234 mechanisms that can bring about a change in choice bias: one in which the starting
235 point of evidence accumulation moves closer to one of the decision boundaries
236 ('starting point model', Figure 1B) (Mulder, Wagenmakers, Ratcliff, Boekel, &
237 Forstmann, 2012), and one in which the drift rate itself is biased towards one of the
238 boundaries (de Gee et al., 2017) ('drift bias model', see Figure 1C, referred to as drift
239 criterion by Ratcliff and McKoon (2008)). The drift bias parameter is determined by
240 estimating the contribution of an evidence-independent constant added to the drift
241 (Figure 2D). In the two respective models, we freed either the drift bias parameter

242 (db, see Figure 2D) for the two conditions while keeping starting point (z) fixed
243 across conditions (for the drift bias model), or vice versa (for the starting point
244 model). Permitting only one parameter at a time to vary freely between conditions
245 allowed us to directly compare the models without having to penalize either model
246 for the number of free parameters. These alternative models make different
247 predictions about the shape of the RT distributions in combination with the response
248 ratios: a shift in starting point results in more target-present choices particularly for
249 short RTs, whereas a shift in drift bias grows over time, resulting in more target-
250 present choices also for longer RTs (de Gee et al., 2017; Ratcliff & McKoon, 2008;
251 Urai et al., 2018). The RT distributions above and below the evidence accumulation
252 graphs in Figure 1B and 1C illustrate these different effects. In both models, all of the
253 non-bias related parameters (drift rate v, boundary separation a and non-decision
254 time u+w, see Figure 2D) were also allowed to vary by condition.

255 We found that the starting point model provided a worse fit to the data than
256 the drift bias model (starting point model, Bayesian Information Criterion (BIC) =
257 79381; drift bias model, BIC = 79262, Figure 2E, see Methods for details).
258 Specifically, for 15/16 participants, the drift bias model provided a better fit than the
259 starting point model, for 12 of which Δ BIC > 6, indicating strong evidence in favor
260 of the drift bias model. Despite the lower BIC for the drift bias model, however, we
261 note that to the naked eye both models provide similarly reasonable fits to the single
262 participant RT distributions (Figure 2—figure supplement 3). Finally, we compared
263 these two models to a model in which both drift bias and starting point were fixed
264 across the conditions, while still allowing the non-bias-related parameters to vary per
265 condition. This model provided the lowest goodness of fit (Δ BIC > 6 for both
266 models for all participants).

267 Given the superior performance of the drift bias model (in terms of BIC), we
268 further characterized decision making under the bias manipulation using parameter
269 estimates from this model, but we come back to the implausibility of the starting point
270 model further below when inspecting the lack of pre-stimulus baseline effects in
271 sensory or motor cortex. Drift rate, reflecting the participants' ability to discriminate
272 targets and nontargets, was somewhat higher in the conservative compared to the
273 liberal condition (liberal: $v = 2.39$ (s.d. 1.07), versus conservative: $v = 3.06$ (s.d.
274 1.16), $p = 0.0001$, permutation test, Figure 2F, left bars). Almost perfect correlations
275 across participants in both conditions between DDM drift rate and SDT d' provided
276 strong evidence that the drift rate parameter captures perceptual sensitivity (liberal, r
277 $= 0.98$, $p = 1e^{-10}$; conservative, $r = 0.96$, $p = 5e^{-9}$, see Figure 2—figure supplement
278 2A).

279 Regarding the DDM bias parameters, the condition-fixed starting point
280 parameter in the drift bias model was smaller than half the boundary separation (i.e.
281 closer to the target-absent boundary ($z = 0.24$ (s.d. 0.06), $p < 0.0001$, tested against
282 0.5)), indicating an overall conservative starting point across conditions (Figure 2—
283 figure supplement 2D), in line with the overall positive SDT criterion (see Figure 2C,
284 right panel). Strikingly, however, whereas the drift bias parameter was on average
285 not different from zero in the conservative condition ($db = -0.04$ (s.d. 1.17), $p =$
286 0.90), drift bias was strongly positive in the liberal condition ($db = 2.08$ (s.d. 1.0), $p =$
287 0.0001; liberal vs conservative: $p = 0.0005$; Figure 2F, right bars). The overall
288 conservative starting point combined with a condition-specific neutral drift bias
289 explained the conservative decision bias (as quantified by SDT criterion) in the
290 conservative condition (Figure 2C). Likewise, in the liberal condition, the overall
291 conservative starting point combined with a condition-specific positive drift bias

292 (pushing the drift towards the target-present boundary) explained the neutral bias
293 observed with SDT criterion (c around zero for liberal, see Figure 2C).

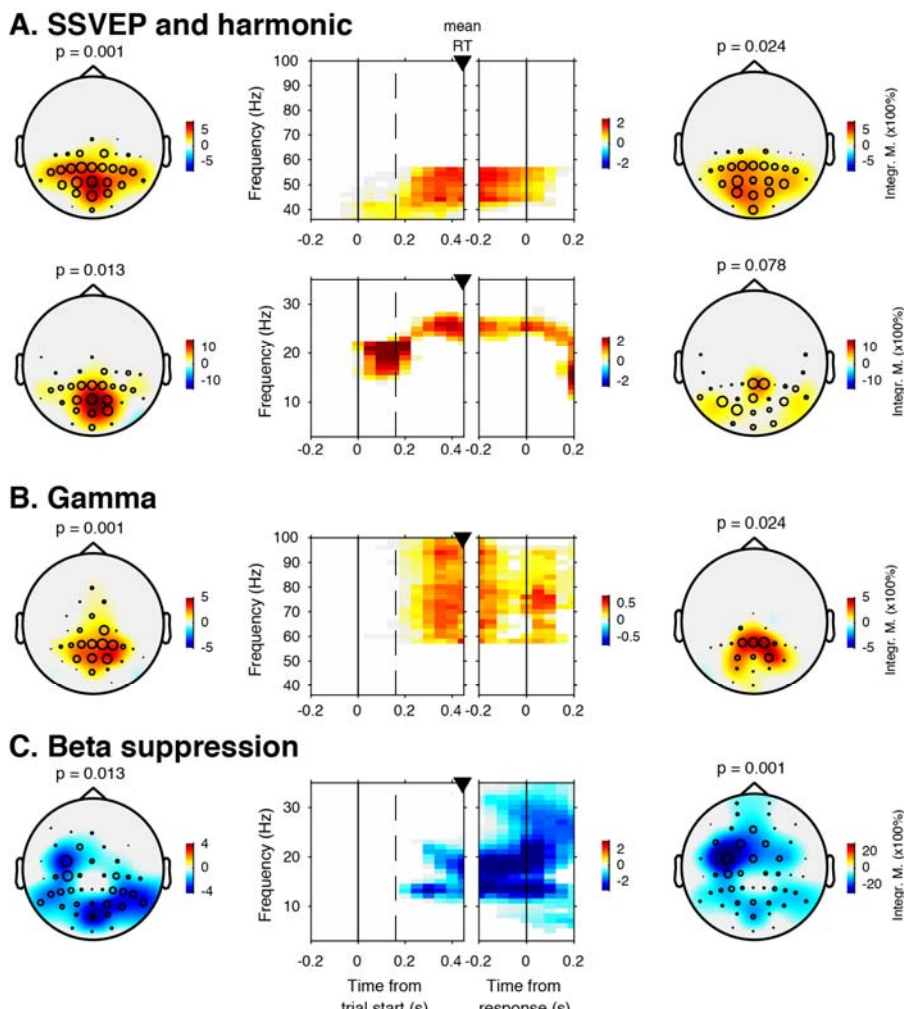
294 Convergent with these modelling results, drift bias was strongly anti-correlated
295 across participants with both SDT criterion ($r = -0.89$ for both conditions, $p = 4e^{-6}$)
296 and average reaction time (liberal, $r = -0.57$, $p = 0.02$; conservative, $r = -0.82$, $p =$
297 $1e^{-4}$, see Figure 2—figure supplement 2B and 2C). The strong correlations between
298 drift rate and d' on the one hand, and drift bias and c on the other, provide
299 converging evidence that the SDT and DDM frameworks capture similar underlying
300 mechanisms, while the DDM additionally captures the dynamic nature of perceptual
301 decision making by linking the decision bias manipulation to the evidence
302 accumulation process itself. As a control, we also correlated starting point with
303 criterion, and found that the correlations were less strong in both conditions (liberal, r
304 = -0.75 ; conservative, $r = -0.77$), suggesting that the drift bias parameter better
305 captured decision bias as instantiated by SDT.

306 Finally, the bias manipulation also affected two other parameters in the drift
307 bias model that were not directly related to sensory evidence accumulation:
308 boundary separation was slightly but reliably higher during the liberal compared to
309 the conservative condition ($p < 0.0001$), and non-decision time (comprising time
310 needed for sensory encoding and motor response execution) was shorter during
311 liberal ($p < 0.0001$) (Figure 2—figure supplement 2D). In conclusion, the drift bias
312 variant of the drift diffusion model best explained how participants adjusted to the
313 decision bias manipulations. In the next sections, we used spectral analysis of the
314 concurrent EEG recordings to identify a plausible neural mechanism that implements
315 biased sensory evidence accumulation.

316

317 **Task-relevant textures induce stimulus-related responses in visual cortex**

318 Sensory evidence accumulation in a visual target detection task presumably relies
319 on stimulus-related signals processed in visual cortex. Such stimulus-related signals
320 are typically reflected in cortical population activity exhibiting a rhythmic temporal
321 structure (Buzsáki & Draguhn, 2004). Specifically, bottom-up processing of visual
322 information has previously been linked to increased high-frequency (> 40 Hz, i.e.
323 gamma) electrophysiological activity over visual cortex (Bastos et al., 2015;
324 Michalareas et al., 2016; Popov et al., 2017; van Kerkoerle et al., 2014). Figure 3
325 shows significant electrode-by-time-by-frequency clusters of stimulus-locked EEG
326 power with respect to the condition-specific pre-trial baseline period (−0.4 to 0 s). We
327 observed a total of four distinct stimulus-related modulations, which emerged after
328 target onset and waned around the time of response: two in the high-frequency
329 range (> 36 Hz, Figures 3A and 3C) and two in the low-frequency range (< 36 Hz,
330 Figures 3B and 3D). First, we found a spatially focal modulation in a narrow
331 frequency range around 25 Hz reflecting the steady state visual evoked potential
332 (SSVEP) arising from entrainment by the visual stimulation frequency of our
333 experimental paradigm (Figure 3A, bottom panel), as well as a second modulation
334 from 42—58 Hz comprising the SSVEP's harmonic (Figure 3A, top panel). Both
335 SSVEP frequency modulations have a similar topographic distribution (see left
336 panels of Figure 3A).



337

338 **Figure 3 | EEG power modulations related to stimulus processing and motor response.** Each
339 panel row depicts a three-dimensional (electrodes-by-time-by-frequency) cluster of power modulation,
340 time-locked both to trial onset (left two panels) and button press (right two panels). Power
341 modulations outside of the significant clusters is masked out. Modulations were computed as the
342 percent signal change from the condition-specific pre-stimulus period (-0.4 to 0 s) and averaged
343 across conditions. Topographical scalp maps show spatial extent of clusters by integrating modulation
344 over time-frequency bins. Time-frequency representations (TFRs) show modulation integrated over
345 electrodes indicated by black circles in the scalp maps. Circle sizes indicate electrode weight in terms
346 of proportion of time-frequency bins contributed to the TFR. P-values above scalp maps indicate
347 multiple comparison-corrected cluster significance using a permutation test across participants (N =
348 14). Solid vertical lines indicate the time of trial onset (left) or button press (right), dotted vertical lines
349 indicate time of (non)target onset. Integr. M., integrated power modulation. **A (Top)** 42-58 Hz (SSVEP

350 harmonic) cluster. **A (Bottom)**. Posterior 23–27 Hz (SSVEP) cluster. **B**. Posterior 59–100 Hz
351 (gamma) cluster. The clusters in A (Top) and B were part of one large cluster (hence the same p-
352 value), and were split based on the sharp modulation increase precisely in the 42–58 Hz range. **C**.
353 12–35 Hz (beta) suppression cluster located more posteriorly aligned to trial onset, and more left-
354 centrally when aligned to button press.

355

356 Third, we observed a 59–100 Hz (gamma) power modulation (Figure 3B),
357 after carefully controlling for high-frequency EEG artifacts due to small fixational eye
358 movements (microsaccades) by removing microsaccade-related activity from the
359 data (Hassler, Trujillo-Barreto, & Gruber, 2011; Hipp & Siegel, 2013; Yuval-
360 Greenberg, Tomer, Keren, Nelken, & Deouell, 2008), and by suppressing non-neural
361 EEG activity through scalp current density (SCD) transformation (Melloni,
362 Schwiedrzik, Wibral, Rodriguez, & Singer, 2009; Perrin, Pernier, Bertrand, &
363 Echallier, 1989) (see Methods for details). Importantly, the topography of the
364 observed gamma modulation was confined to posterior electrodes, in line with a role
365 of gamma in bottom-up processing in visual cortex (Ni et al., 2016). Finally, we
366 observed suppression of low-frequency beta (11–22 Hz) activity in posterior cortex,
367 which typically occurs in parallel with enhanced stimulus-induced gamma activity
368 (Donner & Siegel, 2011; Kloosterman et al., 2015; Meindertsma, Kloosterman, Nolte,
369 Engel, & Donner, 2017; Werkle-Bergner et al., 2014)(Figure 3C). Response-locked,
370 this cluster was most pronounced over left motor cortex (electrode C4), plausibly due
371 to the right-hand button press that participants used to indicate target detection
372 (Donner, Siegel, Fries, & Engel, 2009). In the next sections, we characterize these
373 signals separately for the two conditions, investigating stimulus-related signals within
374 a pooling of eleven occipito-parietal electrodes based on the gamma enhancement
375 in Figure 3B (Oz, POz, Pz, PO3, PO4, and P1 to P6), and motor-related signals in

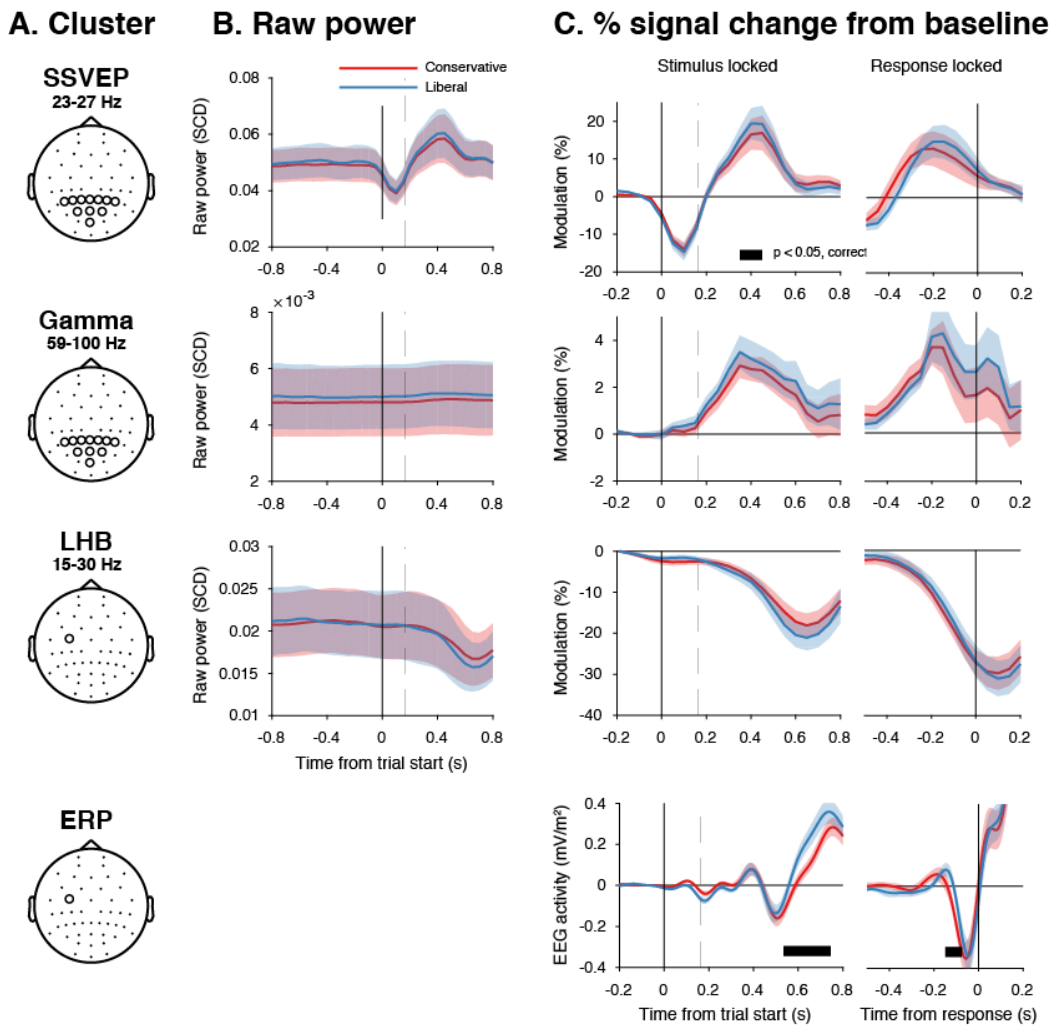
376 left-hemispheric beta (LHB) suppression in electrode C4 (Figure 3C) (O'Connell,
377 Dockree, & Kelly, 2012).

378

379 **EEG power modulation time courses consistent with the drift bias model**

380 Our behavioral results suggest that participants biased sensory evidence
381 accumulation in the liberal condition, rather than changing its starting point. We next
382 sought to provide converging evidence for this conclusion by looking at pre-stimulus
383 activity, post-stimulus activity, and motor-related EEG activity. Following previous
384 studies, we hypothesized that a starting point bias would be reflected in a difference
385 in pre-motor baseline activity between conditions before onset of the decision
386 process (Afacan-Seref, Steinemann, Blangero, & Kelly, 2018; de Lange, Rahnev,
387 Donner, & Lau, 2013), and/or in a difference in pre-stimulus activity such as seen in
388 bottom up stimulus-related SSVEP and gamma power signals (Figure 4A shows the
389 relevant clusters as derived from Figure 3). Thus, we first investigated the timeline of
390 raw power in the SSVEP, gamma and LHB range between conditions (see Figure
391 4B). None of these markers showed a meaningful difference in pre-stimulus baseline
392 activity. Statistically comparing the raw pre-stimulus activity between liberal and
393 conservative in a baseline interval between -0.4 to 0 s prior to trial onset yielded $p =$
394 0.52, $p = 0.51$ and $p = 0.91$, permutation tests, for the respective signals. This
395 confirms a highly similar starting point of evidence accumulation in all these signals.
396 Next, we predicted that a shift in drift bias would be reflected in a steeper slope of
397 post-stimulus ramping activity (leading up to the decision). We reasoned that the
398 best way of ascertaining such an effect would be to baseline the activity to the
399 interval prior to stimulus onset (using the interval between -0.4 to 0 s), such that any
400 post-stimulus effect we find cannot be explained by pre-stimulus differences (if any).

401 The time course of post-stimulus and response-locked activity after baselining can
402 be found in Figure 4C. All three signals showed diverging signals between the liberal
403 and conservative condition after trial onset, consistent with adjustments in the
404 process of evidence accumulation itself. Specifically, we observed higher peak
405 modulation levels for the liberal condition in all three stimulus-locked signals ($p =$
406 0.08, $p = 0.002$ and $p = 0.023$, permutation tests for the respective signals), and
407 found a steeper slope towards the button press for LHB ($p = 0.04$). Finally, the event
408 related potential in motor cortex also showed a steeper slope towards report for
409 liberal ($p = 0.07$, Figure 4, bottom row, baseline plot is not meaningful for time-
410 domain signals due to mean removal during preprocessing). Taken together, these
411 findings provide converging evidence that participants implemented a liberal decision
412 bias by adjusting the rate of evidence accumulation towards the target-present
413 choice boundary, but not its starting point. In the next sections, we sought to identify
414 a neural mechanism that could underlie these biases in the rate of evidence
415 accumulation.



416

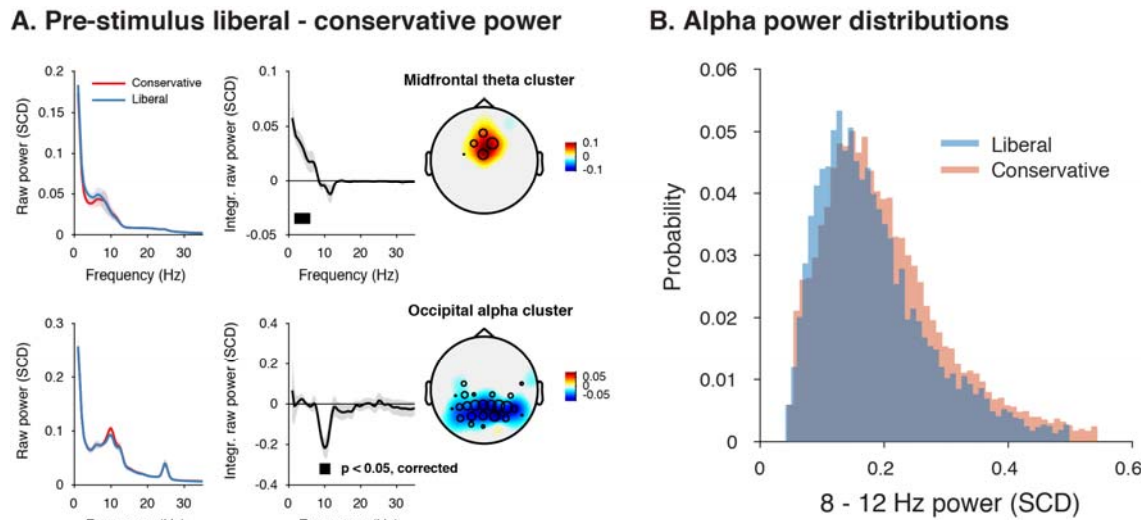
417 **Figure 4 | Experimental task manipulations affect the time course of stimulus- and motor-**
418 **related EEG signals, but not its starting point.** Raw power throughout the baseline period and time
419 courses of power modulation time-locked to trial start and button press. **A.** Relevant electrode clusters
420 and frequency ranges (from Figure 3): Posterior SSVEP, Posterior gamma and Left-hemispheric beta
421 (LHB). **B.** The time course of raw power in a wide interval around the stimulus -0.8 to 0.8 s ms for
422 these clusters. **C.** Stimulus locked and response locked percent signal change from baseline
423 (baseline period: $[-400,0]$ ms). Error bars, SEM. Black horizontal bar indicates significant difference
424 between conditions, cluster-corrected for multiple comparison ($p < 0.05$, two sided).

425

426 **Liberal bias is reflected in pre-stimulus midfrontal theta enhancement and**
427 **posterior alpha suppression**

428 Given a lack of pre-stimulus (starting-point) differences in specific frequency ranges
429 involved in stimulus processing or motor responses (Figure 4B), we next focused on
430 other pre-stimulus differences that might be the root cause of the post-stimulus
431 differences we observed in Figure 4C. To identify such signals, we computed
432 spectral power in the pre-stimulus time window from -1 and 0 s and ran a cluster-
433 based permutation test across all electrodes and frequencies in the low-frequency
434 domain (1–35Hz), looking for power modulations due to our experimental
435 manipulations. Pre-stimulus spectral power indeed uncovered two distinct
436 modulations in the liberal compared to the conservative condition: (1) theta
437 modulation in midfrontal electrodes and (2) alpha modulation in posterior electrodes.
438 Figure 5A depicts the difference between the liberal and conservative condition,
439 confirming significant clusters ($p < 0.05$, cluster-corrected for multiple comparisons)
440 of enhanced theta (2–6 Hz) in frontal electrodes (Fz, Cz, FC1, and FC2), as well as
441 suppressed alpha (8–12 Hz) in a group of posterior electrodes, including all eleven
442 electrodes selected previously based on post-stimulus gamma modulation (Figure
443 3). The two modulations were uncorrelated across participants ($r = 0.06$, $p = 0.82$),
444 suggesting they reflect different neural processes related to our experimental task
445 manipulations. Taken together, these findings show that a strategic liberal bias shift
446 results in increased tonic midfrontal theta as well as suppression of pre-stimulus
447 alpha power. These findings are consistent with literature pointing to a role of
448 midfrontal theta as a source of cognitive control signals originating from pre-frontal
449 cortex (M. X. Cohen & Frank, 2009; van Driel, Ridderinkhof, & Cohen, 2012) and
450 alpha in posterior cortex reflecting spontaneous trial-to-trial fluctuations in decision
451 bias (Iemi et al., 2017). The fact that these pre-stimulus effects occur as a function of
452 our experimental manipulation suggests that they are a hallmark of strategic bias

453 adjustment, rather than a mere correlate of spontaneous shifts in decision bias.
454 Importantly, this finding implies that humans are able to actively control pre-stimulus
455 alpha power in visual cortex (possibly through top-down signals from frontal cortex),
456 plausibly acting to bias sensory evidence accumulation towards the response
457 alternative that maximizes rewards.



458
459 **Figure 5 | Adopting a liberal decision bias is reflected in increased midfrontal theta and**
460 **suppressed pre-stimulus alpha power. A.** Significant clusters of power modulation between liberal
461 and conservative in a pre-stimulus window between -1 and 0 s before trial onset. When performing
462 cluster-based permutation test over frequency (1-35 Hz) and all electrodes, two significant clusters
463 emerged: theta (2-6 Hz, top), and alpha (8-12 Hz, bottom). Left panels: raw power spectra of pre-
464 stimulus neural activity for conservative and liberal separately in the significant clusters (for illustration
465 purposes), Middle panels: Liberal – conservative raw power spectrum. Black horizontal bar indicates
466 statistically significant frequency range ($p < 0.05$, cluster-corrected for multiple comparisons, two-
467 sided). Right panels: Corresponding liberal – conservative scalp topographic maps of the pre-stimulus
468 raw power difference between conditions for EEG theta power (2-6 Hz) and alpha power (8-12 Hz).
469 Plotting conventions as in Figure 3. Error bars, SEM across participants ($N = 15$). **B.** Probability
470 density distributions of single trial alpha power values for both conditions, averaged across
471 participants.

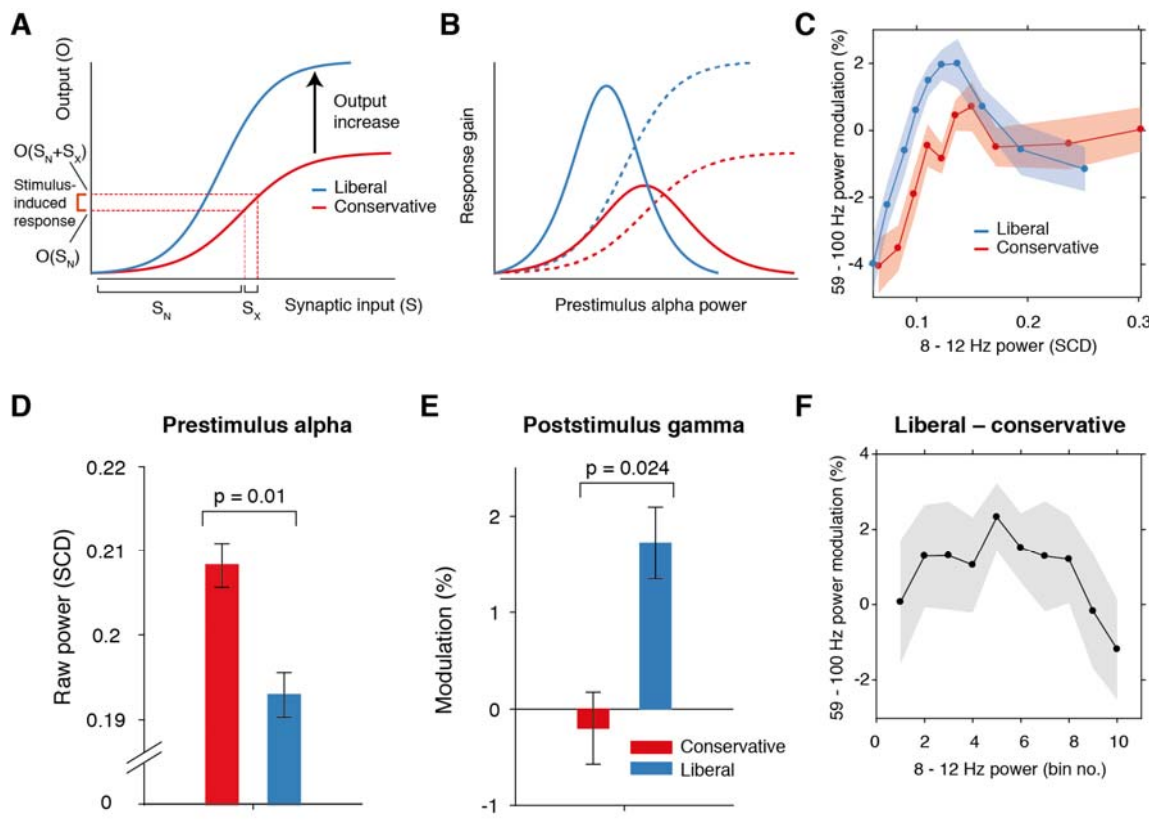
472

473 **Pre-stimulus alpha power mediates cortical gamma responses**

474 Next, we asked how suppression of pre-stimulus alpha activity might bias the
475 process of sensory evidence accumulation. One possibility is that alpha suppression
476 influences evidence accumulation by modulating the susceptibility of visual cortex to
477 sensory stimulation, a phenomenon dubbed ‘neural excitability’ (Iemi et al., 2017;
478 Jensen & Mazaheri, 2010). We explored this possibility using a theoretical response
479 gain model coined by Rajagovindan and Ding (2011). This model postulates that the
480 relationship between the total synaptic input activity that a neuronal ensemble
481 receives and the total output activity it produces is characterized by a sigmoidal
482 function (red line in Figure 6A) – a notion that is biologically plausible (Destexhe,
483 Rudolph, Fellous, & Sejnowski, 2001; Freeman, 1979). In this model, the total
484 synaptic input into visual cortex consists of two components: (1) sensory input (i.e.
485 due to sensory stimulation) and (2) ongoing fluctuations in endogenously generated
486 (i.e. not sensory-related) neural activity. In our experiment, the sensory input into
487 visual cortex can be assumed to be identical across trials, because the same
488 sensory stimulus was presented in each trial (see Figure 2A). The endogenous input,
489 in contrast, is thought to vary from trial to trial reflecting fluctuations in top-down
490 cognitive processes such as attention. These fluctuations are assumed to be
491 reflected in alpha power suppression, such that weaker alpha is associated with
492 increased attention and stronger sensory responses (Figure 6B). Given the
493 combined constant sensory and variable endogenous input in each trial (see
494 horizontal axis in Figure 6A), the strength of the output responses of visual cortex
495 are largely determined by the trial-to-trial variations in alpha strength (see vertical
496 axis in Figure 6A). Furthermore, the sigmoidal shape of the input-output function
497 results in an effective range in the center of the function’s input side which yields the
498 strongest stimulus-induced output responses since the sigmoid curve there is

499 steepest. Mathematically, the effect of endogenous input on stimulus-induced output
500 responses (see marked interval in Figure 6A) can be expressed as the first order
501 derivative or slope of the sigmoid in Figure 6A, which is referred to as the response
502 gain by Rajagovindan and Ding (2011). This derivative is plotted in Figure 6B (red
503 line) across levels of pre-stimulus alpha power, predicting an inverted-U shaped
504 relationship between alpha and response gain in visual cortex.

505 Regarding our experimental conditions, the model not only predicts that the
506 suppression of pre-stimulus alpha observed in the liberal condition reflects a shift in
507 the operational range of alpha (see Figure 5B), but also that it increases the
508 maximum output of visual cortex (a shift from the red to the blue line in Figure 6A).
509 Therefore, the difference between stimulus conditions is not modeled using a single
510 input-output function, but necessitates an additional mechanism that changes the
511 input-output relationship itself. The exact nature of this mechanism is not known
512 (also see Discussion). Rajagovindan and Ding suggest that top-down mechanisms
513 modulate ongoing prestimulus neural activity to increase the slope of the sigmoidal
514 function, but despite the midfrontal theta activity we observed, this hypothesis is
515 somewhat elusive. We have no means to establish directly whether this relationship
516 exists, and can merely reflect on the fact that this change in the input-output function
517 is necessary to capture condition-specific effects of the input-output relationship,
518 both in the data of Rajagovindan and Ding (2011) and in our own data. Thus, as the
519 operational range of alpha shifts leftwards from conservative to liberal, the upper
520 asymptote in Figure 6A moves upwards such that the total maximum output activity
521 increases. This in turn affects the inverted-U-shaped relationship between alpha and
522 gain in visual cortex (blue line in Figure 6B), leading to a steeper response curve in
523 the liberal condition resembling a Gaussian (bell-shaped) function.



524 **Figure 6 | Pre-stimulus alpha power mediates cortical gamma responses.** **A.** Theoretical
 525 response gain model describing the transformation of stimulus-induced and endogenous input activity
 526 (denoted by S_x and S_N respectively) to the total output activity (denoted by $O(S_x + S_N)$) in visual cortex
 527 by a sigmoidal function. Different operational alpha ranges are associated with input-output functions
 528 with different slopes due to corresponding changes in the total output. **B.** Alpha-mediated output
 529 responses (solid lines) are formalized as the first derivative (slope) of the sigmoidal functions (dotted
 530 lines), resulting in inverted-U (Gaussian) shaped relationships between alpha and gamma, involving
 531 stronger response gain in the liberal than in the conservative condition **C.** Corresponding empirical
 532 data showing gamma modulation (same percent signal change units as in Figure 3) as a function of
 533 alpha bin. The location on the x-axis of each alpha bin was taken as the median alpha of the trials
 534 assigned to each bin and averaged across subjects. **D-F.** Model prediction tests. **D.** Raw pre-stimulus
 535 alpha power for both conditions, averaged across subjects. **E.** Post-stimulus gamma power
 536 modulation for both conditions averaged across the two middle alpha bins (5 and 6) in panel C. **F.**
 537 Liberal – conservative difference between the response gain curves shown in panel C, centered on
 538 alpha bin. Error bars, within-subject SEM across participants ($N = 14$).

540

541 The following source data is available for Figure 6:

542 **Source data 1.** SPSS .sav file containing the data used in panels C, E, and F.

543

544 To investigate sensory response gain across different alpha levels in our data,
545 we used the post-stimulus gamma activity (see Figure 3) as a proxy for alpha-
546 mediated output gain in visual cortex (Bastos et al., 2015; Michalareas et al., 2016;
547 Ni et al., 2016; Popov et al., 2017; van Kerkoerle et al., 2014). We exploited the large
548 number of trials per participant per condition (range 543 to 1391 trials) by sorting
549 each participant's trials into ten equal-sized bins ranging from weak to strong alpha,
550 separately for the two conditions. We then calculated the average gamma power
551 modulation within each alpha bin and finally plotted the participant-averaged gamma
552 across alpha bins for each condition in Figure 6C (see Methods for details). This
553 indeed revealed an inverted-U shaped relationship between alpha and gamma, with
554 a steeper curve for the liberal condition.

555 To assess the model's ability to explain the data, we statistically tested three
556 predictions derived from the model. First, the model predicts overall lower average
557 pre-stimulus alpha power for liberal than for conservative due to the shift in the
558 operational range of alpha. This was confirmed in Figure 6D ($p = 0.01$, permutation
559 test, see also Figures 4B and 4C). Second, the model predicts a stronger gamma
560 response for liberal than for conservative around the peak of the gain curve (the
561 center of the effective alpha range, see Figure 6B), which we indeed observed ($p =$
562 0.024 , permutation test on the average of the middle two alpha bins)(Figure 6E).
563 Finally, the model predicts that the difference between the gain curves (when they
564 are aligned over their effective ranges on the x-axis using alpha bin number, as

565 shown in Figure 6 – figure supplement 1A) also resembles a Gaussian curve (Figure
566 6 – figure supplement 1B). Consistent with this prediction, we observed an
567 interaction effect between condition (liberal, conservative) and bin number (1-10)
568 using a standard Gaussian contrast in a 2-way repeated measures ANOVA ($F(1,13)$
569 = 4.6, $p = 0.051$, partial $\eta^2 = 0.26$). Figure 6F illustrates this finding by showing the
570 difference between the two curves in Figure 6C as a function of alpha bin number
571 (see Figure 6 – figure supplement 1C for the curves of both conditions as a function
572 of alpha bin number). Subsequent separate tests for each condition indeed
573 confirmed a significant U-shaped relationship between alpha and gamma in the
574 liberal condition with a large effect size ($F(1,13) = 7.7$, $p = 0.016$, partial $\eta^2 = 0.37$),
575 but no significant effect in the conservative condition with only a small effect size
576 ($F(1,13) = 1.7$, $p = 0.22$, partial $\eta^2 = 0.12$, one-way repeated measures ANOVA's
577 with factor alpha bin, Gaussian contrast).

578 Taken together, these findings suggest that the alpha suppression observed
579 in the liberal compared to the conservative condition boosted stimulus-induced
580 activity in the liberal condition, which in turn might have indiscriminately biased
581 sensory evidence accumulation towards the target-present decision boundary. In the
582 next section, we investigate a direct link between drift bias and stimulus-induced
583 activity as measured through gamma.

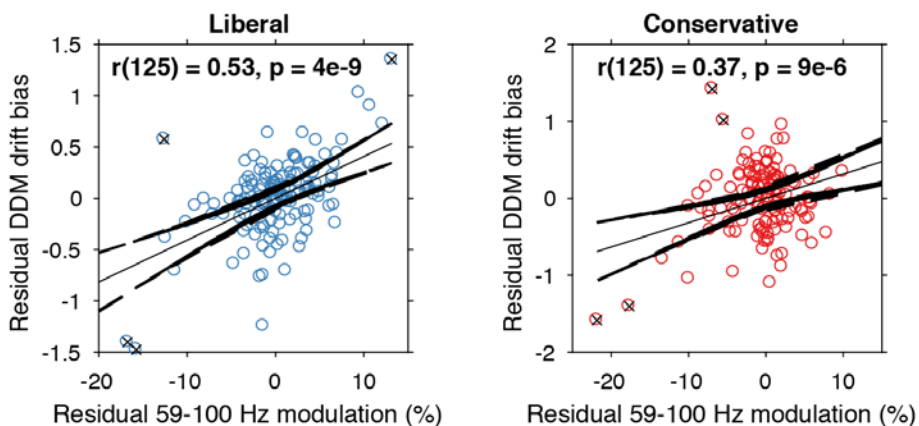
584

585 **Visual cortical gamma activity predicts strength of evidence accumulation bias**
586 The findings presented so far suggest that behaviorally, a liberal decision bias shifts
587 evidence accumulation towards target-present responses (drift bias in the DDM),
588 while neurally it suppresses pre-stimulus alpha while enhancing poststimulus gamma

589 responses. In a final analysis, we asked whether alpha-binned gamma modulation is
590 directly related to a stronger drift bias. To this end, we again applied the drift bias
591 DDM to the behavioral data of each participant, but now freed the drift bias
592 parameter not only for the two conditions, but also for the ten alpha bins for which we
593 calculated gamma modulation (see Figure 6C). We directly tested the
594 correspondence between DDM drift bias and gamma modulation using repeated
595 measures correlation (Bakdash and Marusich, (2017), which takes all repeated
596 observations across participants into account while controlling for non-independence
597 of observations collected within each participant (see Methods for details). Gamma
598 modulation was indeed correlated with drift bias in both conditions (liberal, $r(125) =$
599 0.49, $p = 5e-09$; conservative, $r(125) = 0.38$, $p = 9e-06$) (Figure 7). We tested the
600 robustness of these correlations by excluding the data points that contributed most to
601 the correlations (as determined with Cook's distance) and obtained qualitatively
602 similar results, indicating these correlations were not driven by outliers (Figure 7, see
603 Methods for details). To rule out that starting point could explain this correlation, we
604 repeated this analysis while controlling for the starting point of evidence
605 accumulation estimated per alpha bin within the starting point model. To this end, we
606 regressed both bias parameters on gamma. Crucially, we found that in both
607 conditions starting point bias did not uniquely predict gamma when controlling for
608 drift bias (liberal: $F(1,124) = 5.8$, $p = 0.017$ for drift bias, $F(1,124) = 0.3$, $p = 0.61$ for
609 starting point; conservative: $F(1,124) = 8.7$, $p = 0.004$ for drift bias, $F(1,124) = 0.4$, p
610 = 0.53 for starting point. This finding again suggests that the drift bias model
611 outperforms the starting point model when correlated to gamma power. As a final
612 control, we also performed this analysis for the SSVEP (23–27 Hz) power
613 modulation (see Figure 3B, bottom) and found a similar inverted-U shaped

614 relationship between alpha and the SSVEP for both conditions (Figure 7 – figure
615 supplement 1A), but no correlation with drift bias (liberal, $r(125) = 0.11$, $p = 0.72$,
616 conservative, $r(125) = 0.22$, $p = 0.47$) (Figure 7 – figure supplement 1B) or with
617 starting point (liberal, $r(125) = 0.08$, $p = 0.02$, conservative, $r(125) = 0.22$, $p = 0.95$).
618 This suggests that the SSVEP is similarly coupled to alpha as the stimulus-induced
619 gamma, but is less affected by the experimental conditions and not predictive of
620 decision bias shifts. Taken together, these results suggest that gamma modulation
621 underlies biased sensory evidence accumulation.

622



623

624 **Figure 7 | Alpha-binned gamma modulation correlates with evidence accumulation bias.**

625 Repeated measures correlation between gamma modulation and drift bias for the two conditions.
626 Each circle represents a participant's gamma modulation within one alpha bin. Drift bias and gamma
627 modulation scalars were residualized by removing the average within each participant and condition,
628 thereby removing the specific range in which the participants values operated. Crosses indicate data
629 points that were most influential for the correlation, identified using Cook's distance. Correlations
630 remained qualitatively unchanged when these data points were excluded (liberal, $r(120) = 0.46$, $p =$
631 $8e-07$; conservative, $r(121) = 0.27$, $p = 0.0009$) Error bars, 95% confidence intervals after averaging
632 across participants.

633 The following source data and figure supplements are available for Figure 7:

634 **Source data 1.** MATLAB .mat file containing the data used.

635 **Figure supplement 1.** Alpha-binned post-stimulus SSVEP modulation.

636 Finally, we asked to what extent the enhanced tonic midfrontal theta may have
637 mediated the relationship between alpha-binned gamma and drift bias. To answer
638 this question, we entered drift bias in a 2-way repeated measures ANOVA with
639 factors theta and gamma power (all variables alpha-binned), but found no evidence
640 for mediation of the gamma-drift bias relationship by midfrontal theta (liberal, $F(1,13)$
641 = 1.3, $p = 0.25$; conservative, $F(1,13) = 0.003$, $p = 0.95$). Thus, the enhanced
642 midfrontal theta in the liberal condition plausibly reflects a top-down, attention-related
643 signal indicating the need for cognitive control to avoid missing targets, but its
644 amplitude seemed not directly linked to enhanced sensory evidence accumulation,
645 as found for gamma. This latter finding suggests that the enhanced theta in the
646 liberal condition served as an alarm signal indicating the need for a shift in response
647 strategy, without specifying exactly how this shift was to be implemented (Cavanagh
648 & Frank, 2014).

649

650 **Discussion**

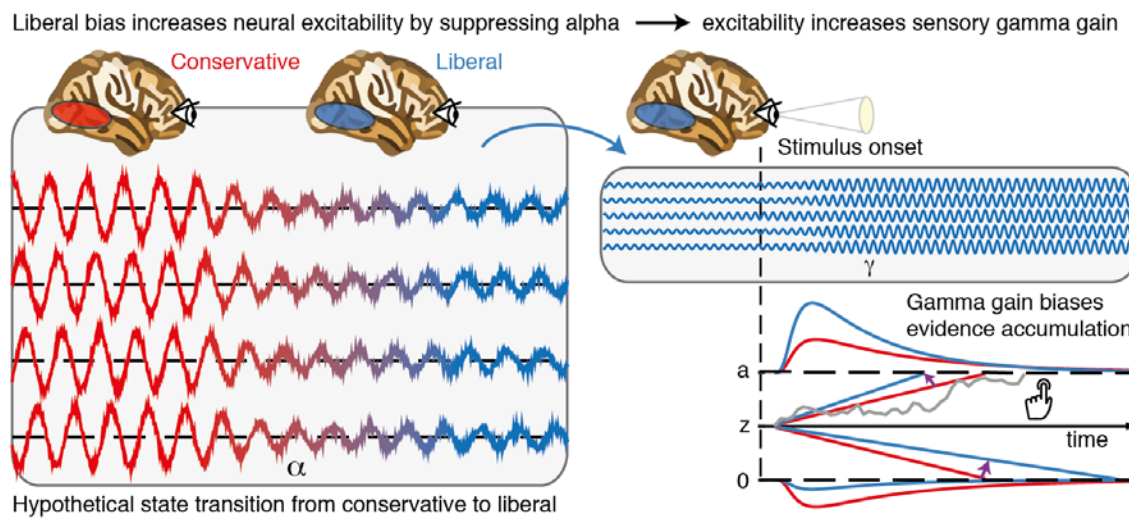
651 Traditionally, bias has been conceptualized in SDT as a criterion threshold that is
652 positioned at an arbitrary location between noise and signal-embedded-in-noise
653 distributions of sensory evidence strengths. The ability to strategically shift decision
654 bias in order to flexibly adapt to stimulus-response reward contingencies in the
655 environment presumably increases chances of survival, but to date such strategic
656 bias shifts as well as their neural underpinnings have not been demonstrated. Here,
657 we compared two versions of the drift diffusion model to show that an experimentally
658 induced bias shift affects the process of sensory evidence accumulation itself, rather
659 than shifting a threshold entity as SDT implies. Moreover, we reveal the neural

660 signature of drift bias by showing that an experimentally induced liberal decision bias
661 is accompanied by changes in midfrontal theta and posterior alpha suppression,
662 resulting in enhanced gamma activity by increased response gain.

663 Although previous studies have shown correlations between suppression of
664 pre-stimulus alpha (8–12 Hz) power and a liberal decision bias during spontaneous
665 fluctuations in alpha activity (Iemi et al., 2017; Limbach & Corballis, 2016), these
666 studies have not established the effect of experimentally induced (within-subject)
667 bias shifts. In the current study, by experimentally manipulating stimulus-response
668 reward contingencies we show for the first time that pre-stimulus alpha can be
669 actively modulated by a participant to achieve changes in decision bias, plausibly
670 mediated by adjusting cognitive control signals originating from midfrontal cortex.
671 Further, we show that alpha suppression in turn modulates gamma activity, in part by
672 increasing the gain of cortical responses. Critically, gamma activity accurately
673 predicted the strength of the drift bias parameter in the DDM drift bias model, thereby
674 providing a direct link between our behavioral and neural findings. Together, these
675 findings show for the first time that humans are able to actively implement decision
676 biases by flexibly adapting neural excitability to strategically shift sensory evidence
677 accumulation towards one of two decision bounds.

678 Based on our results, we propose that decision biases are implemented by
679 flexibly adjusting neural excitability in visual cortex. Figure 8 summarizes this
680 proposed mechanism graphically by visualizing a hypothetical transition in neural
681 excitability following a strategic liberal bias shift, as reflected in visual cortical alpha
682 suppression (left panel). This increased excitability translates into stronger gamma-
683 band responses following stimulus onset (right panel, top). These increased gamma
684 responses finally bias evidence accumulation towards the target-present decision

685 boundary during a liberal state, resulting in more target-present responses, whereas
686 target-absent responses are decimated (blue RT distributions; right panel, bottom).
687 Our experimental manipulation of decision bias in different blocks of trials suggests
688 that decision makers are able to control this biased evidence accumulation
689 mechanism willfully by adjusting cognitive control signals in frontal cortex, which in
690 turn might have a top-down effect on alpha in visual cortex.



691
692 **Figure 8 | Illustrative graphical depiction of the excitability state transition from conservative**
693 **to liberal, and subsequent biased evidence accumulation under a liberal bias.** The left panel
694 shows the transition from a conservative to a liberal condition block. The experimental induction of a
695 liberal decision bias causes alpha suppression in visual cortex, which increases neural excitability.
696 The right top panel shows increased gamma gain for incoming sensory evidence under conditions of
697 high excitability. The right bottom panel shows how increased gamma-gain causes a bias in the drift
698 rate, resulting in more 'target present' responses than in the conservative state.

699

700 A neural mechanism that could underlie bias-related alpha suppression may
701 be under control of the catecholaminergic neuromodulatory systems, consisting of
702 the noradrenaline-releasing locus coeruleus (LC) and dopamine systems (Aston-
703 Jones & Cohen, 2005). These systems are able to modulate the level of arousal and

704 neural gain, and show tight links with pupil responses (de Gee et al., 2017; de Gee,
705 Knapen, & Donner, 2014; Joshi, Li, Kalwani, & Gold, 2015; McGinley, David, &
706 McCormick, 2015). Accordingly, pre-stimulus alpha power suppression has also
707 recently been linked to pupil dilation (Meindertsma et al., 2017). From this
708 perspective, our results reconcile previous studies showing relationships between a
709 liberal bias, suppression of spontaneous alpha power and increased pupil size.
710 Consistent with this, a recent monkey study observed increased neural activity
711 during a liberal bias in the superior colliculus (Crapse, Lau, & Basso, 2018), a mid-
712 brain structure tightly interconnected with the LC (Joshi et al., 2015). Taken together,
713 a more liberal within-subject bias shift (following experimental instruction and/or
714 reward) might activate neuromodulatory systems that subsequently increase cortical
715 excitability and enhance sensory responses for both stimulus and 'noise' signals in
716 visual cortex, thereby increasing a person's propensity for target-present responses
717 (Iemi et al., 2017).

718 We note that although the gain model is consistent with our data as well as
719 the data on which the model was conceived (see Rajagovindan & Ding, 2011), we do
720 not provide a plausible mechanism that could bring about the steepening in the U-
721 curved function observed in Figures 6C and 6F. Although Rajagovindan and Ding
722 report a simulation in their paper suggesting that increased excitability could indeed
723 cause increased gain, this shift could in principle either be caused by the alpha
724 suppression itself, by the same signal that causes alpha suppression, or it could
725 originate from an additional top-down signal from frontal brain regions. Our analysis
726 of pre-stimulus signals indeed shows preliminary evidence for such a top-down
727 signal, but how exactly the gain enhancement comes about remains an open
728 question that should be addressed in future research.

729 Whereas we report a unique link between alpha-mediated gamma modulation
730 and decision bias through the gain model, several previous studies have reported a
731 link between alpha and objective performance instead of bias, particularly in the
732 phase of alpha oscillations (Busch, Dubois, & VanRullen, 2009; Mathewson, Gratton,
733 Fabiani, Beck, & Ro, 2009). Our findings can be reconciled with those by considering
734 that detection sensitivity in many previous studies was often quantified in terms of
735 raw stimulus detection rates, which do not dissociate objective sensitivity from
736 response bias (see Figure 2B) (Green & Swets, 1966). Indeed, our findings are in
737 line with recently reported links between decision bias and spontaneous fluctuations
738 in excitability (Iemi et al., 2017; Iemi & Busch, 2017; Limbach & Corballis, 2016),
739 suggesting an active role of neural excitability in decision bias.

740 Further, one could ask whether the observed change in cortical excitability
741 may reflect a change in target detection sensitivity (drift rate) rather than an
742 intentional bias shift. This is unlikely because that would predict effects opposite to
743 those we observed. We found increased excitability in the liberal condition compared
744 to the conservative condition; if this were related to improved detection performance,
745 one would predict higher sensitivity in the liberal condition, while we found higher
746 sensitivity in the conservative condition (compare drift rate to drift bias in both
747 conditions in Fig. 2C). This finding convincingly ties cortical excitability in our
748 paradigm to decision bias, as opposed to detection sensitivity. Convergently, other
749 studies also report a link between pre-stimulus low-frequency EEG activity and
750 subjective perception, but not objective task performance (Benwell et al., 2017; Iemi
751 & Busch, 2017).

752 In summary, our results suggest that stimulus-induced responses are boosted
753 during a liberal decision bias due to increased cortical excitability, in line with recent

754 work linking alpha power suppression to response gain (Peterson & Voytek, 2017).
755 Future studies can now establish whether this same mechanism is at play in other
756 subjective aspects of decision-making, such as confidence and meta-cognition
757 (Fleming, Putten, & Daw, 2018; Samaha et al., 2017) as well as in a dynamically
758 changing environment (Norton, Fleming, Daw, & Landy, 2017). Explicit manipulation
759 of cortical response gain during a bias manipulation (by pharmacological
760 manipulation of the noradrenergic LC-NE system; (Servan-Schreiber, Printz, &
761 Cohen, 1990)) or by enhancing occipital alpha power using transcranial brain
762 stimulation (Zaehle, Rach, & Herrmann, 2010) could further establish the underlying
763 neural mechanisms involved in decision bias.

764 In the end, although one may be unaware, every decision we make is
765 influenced by biases that operate on one's noisy evidence accumulation process.
766 Understanding how these biases affect our decisions is crucial to enable us to
767 control or invoke them adaptively (Pleskac, Cesario, & Johnson, 2017). Pinpointing
768 the neural mechanisms underlying bias in the current elementary perceptual task
769 may pave the way for understanding how more abstract and high-level decisions are
770 modulated by decision bias (Tversky & Kahneman, 1974).

771

772 **Acknowledgments**

773 The authors thank Timothy J. Pleskac for discussion.

774

775 **Declaration of Interests**

776 The authors declare no competing interests.

777

778 **Data and code sharing**

779 The data analyzed in this study are publicly available on Figshare (Kloosterman et
780 al., 2018). Analysis scripts are publicly available on Github (Kloosterman, 2018).

781

782 **Source data and figure supplements**

783 The following source data and figure supplements are included in this article:

784 Figure 2 – Source data 1. (source_Figure2.mat.zip)

785 Figure 2 – Figure supplements 1, 2 and 3.

786 Figure 6 – Source data 1. (source_Figure6.sav.zip)

787 Figure 6 – Figure supplement 1

788 Figure 7 – Source data 1. (source_Figure7.mat.zip)

789 Figure 7 – Figure supplement 1.

790

791 **Figure supplement legends**

792 **Figure 2—figure supplement 1** | Behavioral and neurophysiological evidence that participants were
793 sensitive to the implicit task structure. **A.** Participant-average RT distributions for hits and false alarms
794 in both conditions. The presence of similar RT distributions for false alarms and hits indicates that
795 participants were sensitive to trial onset despite the fact that trial onsets were only implicitly signaled.
796 Error bars, SEM. **B.** Time-frequency representations of low-frequency EEG power modulations with
797 respect to the pre-stimulus period (−0.4 – 0 s), pooled across the two conditions. Significant low-
798 frequency modulation occurred even for nontarget trials without overt response (correct rejections),
799 indicating that participants detected the onset of a trial even when neither a target was presented nor
800 a response was given. Saturated colors indicate clusters of significant modulation, cluster threshold p

801 < 0.05, two-sided permutation test across participants, cluster-corrected; N = 15). Solid and dotted
802 vertical lines respectively indicate the onset of the trial and the target stimulus. M, power modulation.
803

804 **Figure 2—figure supplement 2 | Signal-detection-theoretic (SDT) behavioral measures during**
805 **both conditions correspond closely to drift diffusion modeling (DDM) parameters. A.** Across-
806 participant Pearson correlation between d' and drift rate for the two conditions. Each dot represents a
807 participant. **B.** As A. but for correlation between criterion and DDM drift bias. The correlation is
808 negative due to a lower criterion reflecting a stronger liberal bias. **C.** Left panel, mean reaction times
809 (RT) for hits and false alarms for the two conditions. Middle and right panels, As A. but for correlation
810 between RT for hits and drift bias. **D.** Parameter estimates in the drift bias DDM not related to
811 evidence accumulation (drift rate). *** p < 0.001; n.s., not significant.

812
813 **Figure 2—figure supplement 3 | Single-participant drift diffusion model fits for the drift bias**
814 **and starting point models for both conditions.** Rows, single participant RT distributions and drift
815 diffusion model fits for the two models for both conditions.

816
817 **Figure 6 – figure supplement 1 | Gain model predictions and corresponding empirical data**
818 **plotted as a function of pre-stimulus alpha bin number. A.** Model predictions for both conditions.
819 The gain curve for the liberal condition is steeper than for the conservative condition. Binning trials
820 based on alpha within each condition directly maps the peaks of the gain curves onto each other. **B.**
821 Model prediction for liberal – conservative as a function of alpha bin number. The difference gain
822 curve between the two conditions is again an inverted-U shaped function. **C.** Corresponding empirical
823 data. The plot is identical to Figure 5C, except that the bin number is plotted instead of the actual
824 alpha power for each condition.

825
826 **Figure 7 – figure supplement 1 | Alpha-binned post-stimulus SSVEP modulation. A.** Inverted-U
827 shaped relationship between alpha and SSVEP modulation, computed as the percent signal change
828 23 – 27 Hz power modulation with respect to the pre-stimulus baseline. **B.** Correlations between
829 SSVEP modulation and drift bias for both conditions. These non-significant correlations are overall
830 weaker than for gamma (see Figure 6).

831

832 **References**

833 Afacan-Seref, K., Steinemann, N. A., Blangero, A., & Kelly, S. P. (2018). Dynamic
834 Interplay of Value and Sensory Information in High-Speed Decision Making.
835 *Current Biology*, 0(0). <http://doi.org/10.1016/j.cub.2018.01.071>
836 Aston-Jones, G., & Cohen, J. D. (2005). An integrative theory of locus coeruleus-
837 norepinephrine function: adaptive gain and optimal performance. *Annual Review*
838 *of Neuroscience*, 28(1), 403–450.
839 <http://doi.org/10.1146/annurev.neuro.28.061604.135709>

840 Bakdash, J. Z., & Marusich, L. R. (2017). Repeated Measures Correlation. *Frontiers*
841 *in Psychology*, 8, 491. <http://doi.org/10.3389/fpsyg.2017.00456>

842 Bastos, A. M., Vezoli, J., Bosman, C. A., Schoffelen, J.-M., Oostenveld, R., Dowdall,
843 J. R., et al. (2015). Visual Areas Exert Feedforward and Feedback Influences
844 through Distinct Frequency Channels. *Neuron*, 85(2), 390–401.
845 <http://doi.org/10.1016/j.neuron.2014.12.018>

846 Benwell, C. S. Y., Tagliabue, C. F., Veniero, D., Cecere, R., Savazzi, S., & Thut, G.
847 (2017). Pre-stimulus EEG power predicts conscious awareness but not objective
848 visual performance. *eNeuro*, 4(6), ENEURO.0182–17.2017.
849 <http://doi.org/10.1523/ENEURO.0182-17.2017>

850 Bogacz, R., Brown, E., Moehlis, J., Holmes, P., & Cohen, J. D. (2006). The physics
851 of optimal decision making: A formal analysis of models of performance in two-
852 alternative forced-choice tasks. *Psychological Review*, 113(4), 700–765.
853 <http://doi.org/10.1037/0033-295X.113.4.700>

854 Busch, N. A., Dubois, J., & VanRullen, R. (2009). The Phase of Ongoing EEG
855 Oscillations Predicts Visual Perception. *Journal of Neuroscience*, 29(24), 7869–
856 7876. <http://doi.org/10.1523/JNEUROSCI.0113-09.2009>

857 Buzsáki, G., & Draguhn, A. (2004). Neuronal oscillations in cortical networks.
858 *Science (New York, NY)*, 304(5679), 1926–1929.
859 <http://doi.org/10.1126/science.1099745>

860 Cavanagh, J. F., & Frank, M. J. (2014). Frontal theta as a mechanism for cognitive
861 control. *Trends in Cognitive Sciences*, 18(8), 414–421.
862 <http://doi.org/10.1016/j.tics.2014.04.012>

863 Cohen, M. X., & Frank, M. J. (2009). Neurocomputational models of basal ganglia
864 function in learning, memory and choice. *Behavioural Brain Research*, 199(1),
865 141–156. <http://doi.org/10.1016/j.bbr.2008.09.029>

866 Crapse, T. B., Lau, H., & Basso, M. A. (2018). A Role for the Superior Colliculus in
867 Decision Criteria. *Neuron*, 97(1), 181–194.e6.
868 <http://doi.org/10.1016/j.neuron.2017.12.006>

869 de Gee, J. W., Colizoli, O., Kloosterman, N. A., Knapen, T., Nieuwenhuis, S., &
870 Donner, T. H. (2017). Dynamic modulation of decision biases by brainstem
871 arousal systems. *eLife*, 6, 309. <http://doi.org/10.7554/eLife.23232>

872 de Gee, J. W., Knapen, T., & Donner, T. H. (2014). Decision-related pupil dilation
873 reflects upcoming choice and individual bias. *Proceedings of the National
874 Academy of Sciences of the United States of America*, 111(5), E618–25.
875 <http://doi.org/10.1073/pnas.1317557111>

876 de Lange, F. P., Rahnev, D. A., Donner, T. H., & Lau, H. (2013). Prestimulus
877 oscillatory activity over motor cortex reflects perceptual expectations. *The
878 Journal of Neuroscience : the Official Journal of the Society for Neuroscience*,
879 33(4), 1400–1410. <http://doi.org/10.1523/JNEUROSCI.1094-12.2013>

880 Destexhe, A., Rudolph, M., Fellous, J. M., & Sejnowski, T. J. (2001). Fluctuating
881 synaptic conductances recreate in vivo-like activity in neocortical neurons.
882 *Neuroscience*, 107(1), 13–24. [http://doi.org/10.1016/S0306-4522\(01\)00344-X](http://doi.org/10.1016/S0306-4522(01)00344-X)

883 Donner, T. H., & Siegel, M. (2011). A framework for local cortical oscillation patterns.
884 *Trends in Cognitive Sciences*, 15(5), 191–199.
885 <http://doi.org/10.1016/j.tics.2011.03.007>

886 Donner, T. H., Siegel, M., Fries, P., & Engel, A. K. (2009). Buildup of choice-
887 predictive activity in human motor cortex during perceptual decision making.
888 *Current Biology*, 19(18), 1581–1585. <http://doi.org/10.1016/j.cub.2009.07.066>

889 Efron, B., & Tibshirani, R. (1998). The problem of regions. *The Annals of Statistics*,
890 26(5), 1687–1718. <http://doi.org/10.1214/aos/1024691353>

891 Fahrenfort, J. J., Scholte, H. S., & Lamme, V. A. F. (2007). Masking disrupts
892 reentrant processing in human visual cortex. *Journal of Cognitive Neuroscience*,
893 19(9), 1488–1497.
894 http://doi.org/10.1162/jocn.2007.19.9.1488&url_ctx_fmt=info:ofi/fmt:kev:mtx:ctx&ft_val_fmt=info:ofi/fmt:kev:mtx:journal&rft.atitle=Masking

895 Fahrenfort, J. J., Scholte, H. S., & Lamme, V. A. F. (2008). The spatiotemporal
896 profile of cortical processing leading up to visual perception. *Journal of Vision*,
897 8(1), 12–12. <http://doi.org/10.1167/8.1.12>

898 Fetsch, C. R., Kiani, R., & Shadlen, M. N. (2014). Predicting the Accuracy of a
899 Decision: A Neural Mechanism of Confidence. *Cold Spring Harbor Symposia on*
900 *Quantitative Biology*, 79, 185–197. <http://doi.org/10.1101/sqb.2014.79.024893>

901 Fleming, S. M., Putten, E. J., & Daw, N. D. (2018). Neural mediators of changes of
902 mind about perceptual decisions. *Nature Neuroscience*, 21(4), 617–624.
903 <http://doi.org/10.1038/s41593-018-0104-6>

904 Freeman, W. J. (1979). Nonlinear gain mediating cortical stimulus-response
905 relations. *Biological Cybernetics*, 33(4), 237–247.
906 <http://doi.org/10.1007/BF00337412>

907 Gold, J. I., & Shadlen, M. N. (2007). The neural basis of decision making. *Annual*
908 *Review of Neuroscience*, 30, 535–574.
909 <http://doi.org/10.1146/annurev.neuro.29.051605.113038>

910 Green, D. M., & Swets, J. A. (1966). Signal detection theory and psychophysics.
911 *Society*, 1, 521.

912 Hassler, U., Trujillo-Barreto, N., & Gruber, T. (2011). Induced gamma band
913 responses in human EEG after the control of miniature saccadic artifacts.
914 *NeuroImage*, 57(4), 1411–1421. <http://doi.org/10.1016/j.neuroimage.2011.05.062>

915 Hipp, J. F., & Siegel, M. (2013). Dissociating neuronal gamma-band activity from
916 cranial and ocular muscle activity in EEG. *Frontiers in Human Neuroscience*, 7,
917 338. <http://doi.org/10.3389/fnhum.2013.00338>

918 Iemi, L., & Busch, N. A. (2017). Moment-to-moment fluctuations in neuronal
919 excitability bias subjective perception rather than decision-making. *bioRxiv*,
920 151324. <http://doi.org/10.1101/151324>

921 Iemi, L., Chaumon, M., Crouzet, S. M., & Busch, N. A. (2017). Spontaneous Neural
922 Oscillations Bias Perception by Modulating Baseline Excitability. *The Journal of*
923 *Neuroscience : the Official Journal of the Society for Neuroscience*, 37(4), 807–
924 819. <http://doi.org/10.1523/JNEUROSCI.1432-16.2017>

925 Jensen, O., & Mazaheri, A. (2010). Shaping functional architecture by oscillatory
926 alpha activity: gating by inhibition. *Frontiers in Human Neuroscience*, 4, 186.
927 <http://doi.org/10.3389/fnhum.2010.00186>

928 Joshi, S., Li, Y., Kalwani, R. M., & Gold, J. I. (2015). Relationships between Pupil
929 Diameter and Neuronal Activity in the Locus Coeruleus, Colliculi, and Cingulate
930 Cortex. *Neuron*, 0(0), 221–234. <http://doi.org/10.1016/j.neuron.2015.11.028>

931 Kiani, R., Hanks, T. D., & Shadlen, M. N. (2008). Bounded Integration in Parietal
932 Cortex Underlies Decisions Even When Viewing Duration Is Dictated by the
933 Environment. *Journal of Neuroscience*, 28(12), 3017–3029.
934 <http://doi.org/10.1523/JNEUROSCI.4761-07.2008>

935 Kloosterman, N. A., de Gee, J. W., Werkle-Bergner, M., Lindenberger, U., Garrett, D.
936 D., & Fahrenfort, J. J. (2018). Data from: Humans strategically shift decision bias
937

938 by flexibly adjusting sensory evidence accumulation in visual cortex.
939 <http://doi.org/https://doi.org/10.6084/m9.figshare.6142940>

940 Kloosterman, N. A., Meindertsma, T., Hillebrand, A., van Dijk, B. W., Lamme, V. A.
941 F., & Donner, T. H. (2015). Top-down modulation in human visual cortex predicts
942 the stability of a perceptual illusion. *Journal of Neurophysiology*, 113(4), 1063–
943 1076. <http://doi.org/10.1152/jn.00338.2014>

944 Lamme, V. A. (1995). The neurophysiology of figure-ground segregation in primary
945 visual cortex. *Journal of Neuroscience*, 15(2), 1605–1615.
946 <http://doi.org/10.1523/JNEUROSCI.15-02-01605.1995>

947 Lamme, V. A. F., Zipser, K., & Spekreijse, H. (2006). Masking Interrupts Figure-
948 Ground Signals in V1. *Dx.Doi.org*, 14(7), 1044–1053.
949 <http://doi.org/10.1162/089892902320474490>

950 Limbach, K., & Corballis, P. M. (2016). Prestimulus alpha power influences response
951 criterion in a detection task. *Psychophysiology*, 53(8), 1154–1164.
952 <http://doi.org/10.1111/psyp.12666>

953 Maris, E., & Oostenveld, R. (2007). Nonparametric statistical testing of EEG-and
954 MEG-data. *Journal of Neuroscience Methods*, 164(1), 177–190.
955 <http://doi.org/10.1016/j.jneumeth.2007.03.024>

956 Mathewson, K. E., Gratton, G., Fabiani, M., Beck, D. M., & Ro, T. (2009). To See or
957 Not to See: Prestimulus α Phase Predicts Visual Awareness. *Journal of*
958 *Neuroscience*, 29(9), 2725–2732. <http://doi.org/10.1523/JNEUROSCI.3963-08.2009>

959 McGinley, M. J., David, S. V., & McCormick, D. A. (2015). Cortical Membrane
960 Potential Signature of Optimal States for Sensory Signal Detection. *Neuron*,
961 87(1), 179–192. <http://doi.org/10.1016/j.neuron.2015.05.038>

962 Meindertsma, T., Kloosterman, N. A., Nolte, G., Engel, A. K., & Donner, T. H. (2017).
963 Multiple Transient Signals in Human Visual Cortex Associated with an
964 Elementary Decision. *Journal of Neuroscience*, 37(23), 5744–5757.
965 <http://doi.org/10.1523/JNEUROSCI.3835-16.2017>

966 Melloni, L., Schwiedrzik, C. M., Wibral, M., Rodriguez, E., & Singer, W. (2009).
967 Response to: Yuval-Greenberg et al., “Transient Induced Gamma-Band
968 Response in EEG as a Manifestation of Miniature Saccades.” *Neuron* 58, 429–
969 441. *Neuron*, 62(1), 8–10– author reply 10–12.
970 <http://doi.org/10.1016/j.neuron.2009.04.002>

971 Michalareas, G., Vezoli, J., van Pelt, S., Schoffelen, J.-M., Kennedy, H., & Fries, P.
972 (2016). Alpha-Beta and Gamma Rhythms Subserve Feedback and Feedforward
973 Influences among Human Visual Cortical Areas. *Neuron*, 89(2), 384–397.
974 <http://doi.org/10.1016/j.neuron.2015.12.018>

975 Mitra, P. P., & Pesaran, B. (1999). Analysis of Dynamic Brain Imaging Data.
976 *Biophysical Journal*, 76(2), 691–708. [http://doi.org/10.1016/S0006-3495\(99\)77236-X](http://doi.org/10.1016/S0006-3495(99)77236-X)

977 Mulder, M. J., Wagenmakers, E.-J., Ratcliff, R., Boekel, W., & Forstmann, B. U.
978 (2012). Bias in the brain: a diffusion model analysis of prior probability and
979 potential payoff. *The Journal of Neuroscience : the Official Journal of the Society*
980 *for Neuroscience*, 32(7), 2335–2343. <http://doi.org/10.1523/JNEUROSCI.4156-11.2012>

981 Neath, A. A., & Cavanaugh, J. E. (2012). The Bayesian information criterion:
982 background, derivation, and applications. *Wiley Interdisciplinary Reviews:*
983 *Computational Statistics*, 4(2), 199–203. <http://doi.org/10.1002/wics.199>

987 Ni, J., Wunderle, T., Lewis, C. M., Desimone, R., Diester, I., & Fries, P. (2016).
988 Gamma-Rhythmic Gain Modulation. *Neuron*, 92(1), 240–251.
989 <http://doi.org/10.1016/j.neuron.2016.09.003>

990 Norton, E. H., Fleming, S. M., Daw, N. D., & Landy, M. S. (2017). Suboptimal
991 Criterion Learning in Static and Dynamic Environments. *PLoS Computational
992 Biology*, 13(1), e1005304–28. <http://doi.org/10.1371/journal.pcbi.1005304>

993 O'Connell, R. G., Dockree, P. M., & Kelly, S. P. (2012). A supramodal accumulation-
994 to-bound signal that determines perceptual decisions in humans. *Nature* ...,
995 15(12), 1729–1735. <http://doi.org/10.1038/nature.3248>

996 Oostenveld, R., Fries, P., Maris, E., & Schoffelen, J.-M. (2011). FieldTrip: open
997 source software for advanced analysis of MEG, EEG, and invasive
998 electrophysiological data. *Computational Intelligence and Neuroscience*, 2011(1),
999 1–9. <http://doi.org/10.1155/2011/156869>

1000 Perrin, F., Pernier, J., Bertrand, O., & Echallier, J. F. (1989). Spherical splines for
1001 scalp potential and current density mapping. *Electroencephalography and
1002 Clinical Neurophysiology*, 72(2), 184–187. [http://doi.org/10.1016/0013-4694\(89\)90180-6](http://doi.org/10.1016/0013-4694(89)90180-6)

1003 Peterson, E. J., & Voytek, B. (2017). Alpha oscillations control cortical gain by
1004 modulating excitatory-inhibitory background activity. *Biorxiv.org*
1005 . <http://doi.org/https://doi.org/10.1101/185074>

1006 Pleskac, T. J., Cesario, J., & Johnson, D. J. (2017). How race affects evidence
1007 accumulation during the decision to shoot. *Psychonomic Bulletin & Review*,
1008 18(2), 1–30. <http://doi.org/10.3758/s13423-017-1369-6>

1009 Popov, T., Kastner, S., & Jensen, O. (2017). FEF-Controlled Alpha Delay Activity
1010 Precedes Stimulus-Induced Gamma-Band Activity in Visual Cortex. *Journal of
1011 Neuroscience*, 37(15), 4117–4127. <http://doi.org/10.1523/JNEUROSCI.3015-16.2017>

1012 Rajagovindan, R., & Ding, M. (2011). From prestimulus alpha oscillation to visual-
1013 evoked response: an inverted-U function and its attentional modulation. *Journal
1014 of Cognitive Neuroscience*, 23(6), 1379–1394.
1015 <http://doi.org/10.1162/jocn.2010.21478>

1016 Ratcliff, R. (1978). A theory of memory retrieval. *Psychological Review*, 85(2), 59–
1017 108. <http://doi.org/10.1037/0033-295X.85.2.59>

1018 Ratcliff, R. (2006). Modeling response signal and response time data. *Cognitive
1019 Psychology*, 53(3), 195–237. <http://doi.org/10.1016/j.cogpsych.2005.10.002>

1020 Ratcliff, R., & McKoon, G. (2008). The Diffusion Decision Model: Theory and Data for
1021 Two-Choice Decision Tasks. *Neural Computation*, 20(4), 873–922.
1022 <http://doi.org/10.1162/neco.2008.12-06-420>

1023 Ratcliff, R., Huang-Pollock, C., & McKoon, G. (2016, August 15). Modeling Individual
1024 Differences in the Go/No-Go Task With a Diffusion Model. <http://doi.org/http://dx.doi.org/10.1037/dec0000065>

1025 Samaha, J., Iemi, L., & Postle, B. R. (2017). Prestimulus alpha-band power biases
1026 visual discrimination confidence, but not accuracy. *Consciousness and
1027 Cognition*. <http://doi.org/10.1016/j.concog.2017.02.005>

1028 Servan-Schreiber, D., Printz, H., & Cohen, J. D. (1990). A network model of
1029 catecholamine effects: gain, signal-to-noise ratio, and behavior. *Science (New
1030 York, NY)*, 249(4971), 892–895.

1031 Supèr, H., Spekreijse, H., letters, V. L. N., 2003. (2003). Figure–ground activity in
1032 primary visual cortex (V1) of the monkey matches the speed of behavioral
1033 response. *Elsevier*

1034

1035

1036

1037 , 344(2), 75–78. [http://doi.org/10.1016/S0304-3940\(03\)00360-4](http://doi.org/10.1016/S0304-3940(03)00360-4)

1038 Tversky, A., & Kahneman, D. (1974). Judgment under Uncertainty: Heuristics and
1039 Biases. *Science (New York, NY)*, 185(4157), 1124–1131.
<http://doi.org/10.1126/science.185.4157.1124>

1040 Urai, A. E., de Gee, J. W., & Donner, T. H. (2018). Choice history biases subsequent
1041 evidence accumulation. *bioRxiv*, 251595. <http://doi.org/10.1101/251595>

1042 van Driel, J., Ridderinkhof, K. R., & Cohen, M. X. (2012). Not All Errors Are Alike:
1043 Theta and Alpha EEG Dynamics Relate to Differences in Error-Processing
1044 Dynamics. *Journal of Neuroscience*, 32(47), 16795–16806.
<http://doi.org/10.1523/JNEUROSCI.0802-12.2012>

1045 van Kerkoerle, T., Self, M. W., Dagnino, B., Gariel-Mathis, M.-A., Poort, J., van der
1046 Togt, C., & Roelfsema, P. R. (2014). Alpha and gamma oscillations characterize
1047 feedback and feedforward processing in monkey visual cortex. *Proceedings of
1048 the National Academy of Sciences of the United States of America*, 111(40),
1049 14332–14341. <http://doi.org/10.1073/pnas.1402773111>

1050 Werkle-Bergner, M., Grandy, T. H., Chicherio, C., Schmiedek, F., Lovden, M., &
1051 Lindenberger, U. (2014). Coordinated within-Trial Dynamics of Low-Frequency
1052 Neural Rhythms Controls Evidence Accumulation. *Journal of Neuroscience*,
1053 34(25), 8519–8528. <http://doi.org/10.1523/JNEUROSCI.3801-13.2014>

1054 White, C. N., & Poldrack, R. A. (2014). Decomposing bias in different types of simple
1055 decisions. *Journal of Experimental Psychology Learning, Memory, and
1056 Cognition*, 40(2), 385–398. <http://doi.org/10.1037/a0034851>

1057 Wiecki, T. V., Sofer, I., & Frank, M. J. (2013). HDDM: Hierarchical Bayesian
1058 estimation of the Drift-Diffusion Model in Python. *Frontiers in Neuroinformatics*, 7.
<http://doi.org/10.3389/fninf.2013.00014>

1059 Yuval-Greenberg, S., Tomer, O., Keren, A. S., Nelken, I., & Deouell, L. Y. (2008).
1060 Transient Induced Gamma-Band Response in EEG as a Manifestation of
1061 Miniature Saccades. *Neuron*, 58(3), 429–441.
<http://doi.org/10.1016/j.neuron.2008.03.027>

1062 Zaehle, T., Rach, S., & Herrmann, C. S. (2010). Transcranial Alternating Current
1063 Stimulation Enhances Individual Alpha Activity in Human EEG. *PLoS ONE*,
1064 5(11), e13766. <http://doi.org/10.1371/journal.pone.0013766>

1065

1066

1067

1068

1069

1070

1071 Materials and Methods

1072 Key resources table

Reagent type (species) or resource	Designation	Source or reference	Identifiers	Additional information
biological sample (Humans)	Participants	This paper		See Participants section in Materials and Methods
software,	MATLAB	Mathworks	MATLAB_R2016b,	

algorithm software, algorithm	Presentation	NeuroBS	RRID:SCR_001622 Presentation_v9.9, RRID:SCR_002521	
software, algorithm	Custom analysis code	Kloosterman (2018)	https://github.com/ nkloost1/critEEG	
other	EEG data experimental task	Kloosterman et al.(2018)	https://doi.org/10.6084/ m9.figshare.6142940	

1073

1074 **Participants** Sixteen participants (eight females, mean age 24.1 years, \pm 1.64) took
1075 part in the experiment, either for financial compensation (EUR 10, - per hour) or in
1076 partial fulfillment of first year psychology course requirements. Each participant
1077 completed three experimental sessions on different days, each session lasting ca. 2
1078 hours, including preparation and breaks. One participant completed only two
1079 sessions, yielding a total number of sessions across subjects of 47. Due to technical
1080 issues, for one session only data for the liberal condition was available. One
1081 participant was an author. All participants had normal or corrected-to-normal vision
1082 and were right handed. Participants provided written informed consent before the
1083 start of the experiment. All procedures were approved by the ethics committee of the
1084 University of Amsterdam.

1085 Regarding sample size, our experiment consisted of 16 biological replications
1086 (participants) and either two (one participant) or three (fifteen participants) technical
1087 replications (i.e. experimental sessions). The sample size was determined based on
1088 two criteria: 1) obtaining large amounts of data per participant (thousands of trials),
1089 which is necessary to perform robust drift diffusion modelling of choice behavior and
1090 obtain reliable EEG spectral power estimates for each of the ten bins of trials that
1091 were created within participants, and 2) obtaining data from a sufficient number of

1092 participants to leverage across-subject variability in correlational analyses. Thus, we
1093 emphasized obtaining many data points per participant relative to obtaining many
1094 participants, while still preserving the ability to perform correlations across
1095 participants.

1096 All participants were included in the signal-detection-theoretical and drift
1097 diffusion modeling analyses. One participant was excluded from the EEG analysis
1098 due to excessive noise (EEG power spectrum opposite of 1/frequency). One further
1099 participant was excluded from the analyses that included condition-specific gamma
1100 because the liberal–conservative difference in gamma in this participant was > 3
1101 standard deviations away from the other participants.

1102 **Stimuli** Stimuli consisted of a continuous semi-random rapid serial visual
1103 presentation (rsvp) of full screen texture patterns. The texture patterns consisted of
1104 line elements approx. 0.07° thick and 0.4° long in visual angle. Each texture in the
1105 rsvp was presented for 40 ms (i.e. stimulation frequency 25 Hz), and was oriented in
1106 one of four possible directions: 0° , 45° , 90° or 135° . Participants were instructed to
1107 fixate a red dot in the center of the screen. At random inter trial intervals (ITI's)
1108 sampled from a uniform distribution (ITI range 0.3 – 2.2 s), the rsvp contained a fixed
1109 sequence of 25 texture patterns, which in total lasted one second. This fixed
1110 sequence consisted of four stimuli preceding a (non-)target stimulus (orientations of
1111 45° , 90° , 0° , 90° respectively) and twenty stimuli following the (non)-target
1112 (orientations of 0° , 90° , 0° , 90° , 0° , 45° , 0° , 135° , 90° , 45° , 0° , 135° , 0° , 45° , 90° , 45° ,
1113 90° , 135° , 0° , 135° respectively) (see Figure 2A). The fifth texture pattern within the
1114 sequence (occurring from 0.16 s after sequence onset) was either a target or a
1115 nontarget stimulus. Nontargets consisted of either a 45° or a 135° homogenous
1116 texture, whereas targets contained a central orientation-defined square of 2.42°

1117 visual angle, thereby consisting of both a 45° and a 135° texture. 50% of all targets
1118 consisted of a 45° square and 50% of a 135° square. Of all trials, 75% contained a
1119 target and 25% a nontarget. Target and nontarget trials were presented in random
1120 order. To avoid specific influences on target stimulus visibility due to presentation of
1121 similarly or orthogonally oriented texture patterns temporally close in the cascade, no
1122 45° and 135° oriented stimuli were presented directly before or after presentation of
1123 the target stimulus. All stimuli had an isoluminance of 72.2 cd/m². Stimuli were
1124 created using MATLAB (The Mathworks, Inc., Natick, MA, USA; RRID:SCR_001622)
1125 and presented using Presentation version 9.9 (Neurobehavioral systems, Inc.,
1126 Albany, CA, USA; RRID:SCR_002521).

1127 **Experimental design** The participants' task was to detect and actively report targets
1128 by pressing a button using their right hand. Targets occasionally went unreported,
1129 presumably due to constant forward and backward masking by the continuous
1130 cascade of stimuli and unpredictability of target timing (Fahrenfort, Scholte, &
1131 Lamme, 2007). The onset of the fixed order of texture patterns preceding and
1132 following (non-)target stimuli was neither signaled nor apparent.

1133 At the beginning of the experiment, participants were informed they could
1134 earn a total bonus of EUR 30, -, on top of their regular pay of EUR 10, - per hour or
1135 course credit. In two separate conditions within each session of testing, we
1136 encouraged participants to use either a conservative or a liberal bias for reporting
1137 targets using both aversive sounds as well as reducing their bonus after errors. In
1138 the conservative condition, participants were instructed to only press the button
1139 when they were relatively sure they had seen the target. The instruction on screen
1140 before block onset read as follows: "Try to detect as many targets as possible. Only
1141 press when you are relatively sure you just saw a target." To maximize effectiveness

1142 of this instruction, participants were told the bonus would be diminished by ten cents
1143 after a false alarm. During the experiment, a loud aversive sound was played after a
1144 false alarm to inform the participant about an error. During the liberal condition,
1145 participants were instructed to miss as few targets as possible. The instruction on
1146 screen before block onset read as follows: "Try to detect as many targets as
1147 possible. If you sometimes press when there was nothing this is not so bad". In this
1148 condition, the loud aversive sound was played twice in close succession whenever
1149 they failed to report a target, and three cents were subsequently deducted from their
1150 bonus. The difference in auditory feedback between both conditions was included to
1151 inform the participant about the type of error (miss or false alarm), in order to
1152 facilitate the desired bias in both conditions. After every block, the participant's score
1153 (number of missed targets in the liberal condition and number of false alarms in the
1154 conservative condition) was displayed on the screen, as well as the remainder of the
1155 bonus. After completing the last session of the experiment, every participant was
1156 paid the full bonus as required by the ethical committee.

1157 Participants performed six blocks per session lasting ca. nine minutes each.
1158 During a block, participants continuously monitored the screen and were free to
1159 respond by button press whenever they thought they saw a target. Each block
1160 contained 240 trials, of which 180 target and 60 nontarget trials. The task instruction
1161 was presented on the screen before the block started. The condition of the first block
1162 of a session was counterbalanced across participants. Prior to EEG recording in the
1163 first session, participants performed a 10-minute practice run of both conditions, in
1164 which visual feedback directly after a miss (liberal condition) or false alarm
1165 (conservative) informed participants about their mistake, allowing them to adjust their

1166 decision bias accordingly. There were short breaks between blocks, in which
1167 participants indicated when they were ready to begin the next block.

1168 **Behavioral analysis** We calculated each participant's criterion c (Green & Swets,
1169 1966) across the trials in each condition as follows:

$$c = -\frac{1}{2} [Z(\text{Hit-rate}) + Z(\text{FA-rate})]$$

1170 where hit-rate is the proportion target-present responses of all target-present trials,
1171 false alarm (FA)-rate is the proportion target-present responses of all target-absent
1172 trials, and $Z(\dots)$ is the inverse standard normal distribution. Furthermore, we
1173 calculated objective sensitivity measure d' using:

1174

$$d' = Z(\text{Hit-rate}) - Z(\text{FA-rate})$$

1175

1176 as well as by subtracting hit and false alarm rates. Reaction times (RTs) were
1177 measured as the duration between target onset and button press.

1178 **Drift diffusion modeling of choice behavior** In order to be detected, the 40 ms-
1179 duration figure-ground targets used in our study undergo a process in visual cortex
1180 called figure-ground segregation. This process has been well characterized in man
1181 and monkey (Fahrenfort, Scholte, & Lamme, 2008; Lamme, 1995; Lamme, Zipser, &
1182 Spekreijse, 2006; Supèr, Spekreijse, letters, 2003, 2003), and results from recurrent
1183 processing to extract the surface region in visual cortex. Figure-ground segregation
1184 is known to extend far beyond the mere presentation time of the stimulus, thus
1185 providing a plausible neural basis for the evidence accumulation process. Further, a
1186 central assumption of the drift diffusion model is that the process of evidence

1187 accumulation is gradual, independent of whether sensory input is momentary.
1188 Indeed, the DDM was initially developed to explain reaction time distributions during
1189 memory retrieval, in which evidence accumulation must occur through retrieval of a
1190 memory trace within the brain, in the complete absence of external stimulus at the
1191 time of the decision (Ratcliff, 1978). Our observed RT distributions show the typical
1192 features that occur across many different types of decision and memory tasks, which
1193 the DDM is so well able to capture, including a sharp leading edge and a long tail of
1194 the distributions (see Figure 2-supplement 3). The success of the DDM in fitting
1195 these data is consistent with previous work (e.g. Ratcliff (2006)) and might reflect the
1196 fact that observers modulate the underlying components of the decision process also
1197 when they do not control the stimulus duration (Kiani, Hanks, & Shadlen, 2008).

1198 We fitted the drift diffusion model to our behavioral data for each subject
1199 individually, and separately for the liberal and conservative conditions. We fitted the
1200 model using a G square method based on quantile RT's (RT cutoff, 200 ms, for
1201 details, see Ratcliff et al. (2016)), using a modified version of the HDDM 0.6.0
1202 package (Wiecki, Sofer, & Frank, 2013). The RT distributions for target-present
1203 responses were represented by the 0.1, 0.3, 0.5, 0.7 and 0.9 quantiles, and, along
1204 with the associated response proportions, contributed to G square. In addition, a
1205 single bin containing the number of target-absent responses contributed to G square.
1206 Each model fit was run six times, after which the best fitting run was kept. Fitting the
1207 model to RT distributions for target-present and target-absent choices (termed
1208 'stimulus coding' in Wiecki et al. (2013)), as opposed to the more common fits of
1209 correct and incorrect choice RT's (termed 'accuracy coding' in Wiecki et al. (2013)),
1210 allowed us to estimate parameters that could have induced biases in subjects'
1211 behavior.

1212 Parameter recovery simulations showed that letting both the starting point of
1213 the accumulation process and drift bias (an evidence-independent constant added to
1214 the drift toward one or the other bound) free to vary with experimental condition is
1215 problematic for data with no explicit target-absent responses (data not shown). Thus,
1216 to test whether shifts in drift bias or starting point underlie bias we fitted three
1217 separate models. In the first model ('fixed model'), we allowed only the following
1218 parameters to vary between the liberal and conservative condition: (i) the mean drift
1219 rate across trials; (ii) the separation between both decision bounds (i.e., response
1220 caution); and (iii) the non-decision time (sum of the latencies for sensory encoding
1221 and motor execution of the choice). Additionally, the bias parameters starting point
1222 and drift bias were fixed for the experimental conditions. The second model ('starting
1223 point model') was the same as the fixed model, except that we let the starting point
1224 of the accumulation process vary with experimental condition, whereas the drift bias
1225 was kept fixed for both conditions. The third model ('drift bias model') was the same
1226 as the fixed model, except that we let the drift bias vary with experimental condition,
1227 while the starting point was kept fixed for both conditions. We used Bayesian
1228 Information Criterion (BIC) to select the model which provided the best fit to the data
1229 (Neath & Cavanaugh, 2012). The BIC compares models based on their maximized
1230 log-likelihood value, while penalizing for the number of parameters.

1231 **Distinguishing DDM drift bias and drift rate** In our task, only target-present
1232 responses were coupled to a behavioral response (button-press), so we could
1233 measure reaction times only for these responses, whereas reaction times for target-
1234 absent responses remained implicit. Thus, in our fitting procedure, the RT
1235 distributions for target-present responses were represented by the 0.1, 0.3, 0.5, 0.7
1236 and 0.9 quantiles, and, along with the associated response proportions, contributed

1237 to G square. In addition, a single bin containing the number of target-absent
1238 responses contributed to G square. It has been shown that such a diffusion model
1239 with an implicit (no response) boundary can be fit to data with almost the same
1240 accuracy as fitting the two-choice model to two-choice data (Ratcliff et al., 2016). In a
1241 diffusion model with an implicit (no response) boundary, both an increase in drift rate
1242 and drift criterion would predict faster target-present responses. However, the key
1243 distinction is that an increase in drift additionally predicts more correct responses (for
1244 both target-present and target-absent responses), and an increase in drift criterion
1245 shifts the relative fraction of target-present and target-absent responses (decision
1246 bias). Because a single bin containing the number of target-absent responses
1247 contributed to G square, our fitting procedure can distinguish between decision bias
1248 versus drift rate.

1249 **EEG recording** Continuous EEG data were recorded at 256 Hz using a 48-channel
1250 BioSemi Active-Two system (BioSemi, Amsterdam, the Netherlands), connected to a
1251 standard EEG cap according to the international 10-20 system. Electrooculography
1252 (EOG) was recorded using two electrodes at the outer canthi of the left and right
1253 eyes and two electrodes placed above and below the right eye. Horizontal and
1254 vertical EOG electrodes were referenced against each other, two for horizontal and
1255 two for vertical eye movements (blinks). We used the Fieldtrip toolbox (Oostenveld,
1256 Fries, Maris, & Schoffelen, 2011) and custom software (Kloosterman, 2018) in
1257 MATLAB R2016b (The Mathworks Inc., Natick, MA, USA; RRID:SCR_001622) to
1258 process the data (see below). Data were re-referenced to the average voltage of two
1259 electrodes attached to the earlobes.

1260 **Trial extraction and preprocessing** We extracted trials of variable duration from 1
1261 s before target sequence onset until 1.25 after button press for trials that included a

1262 button press (hits and false alarms), and until 1.25 s after stimulus onset for trials
1263 without a button press (misses and correct rejects). The following constraints were
1264 used to classify (non-)targets as detected (hits and false alarms), while avoiding the
1265 occurrence of button presses in close succession to target reports and button
1266 presses occurring outside of trials: 1) A trial was marked as detected if a response
1267 occurred within 0.84 s after target onset; 2) when the onset of the next target
1268 stimulus sequence started before trial end, the trial was terminated at the next trial's
1269 onset; 3) when a button press occurred in the 1.5 s before trial onset, the trial was
1270 extracted from 1.5 s after this button press; 4) when a button press occurred
1271 between 0.5 s before until 0.2 s after sequence onset, the trial was discarded. See
1272 Kloosterman et al. (2015) and Meindertsma et al. (2017) for similar trial extraction
1273 procedures. After trial extraction, channel time courses were linearly detrended and
1274 the mean of every channel was removed per trial.

1275 **Artifact rejection** Trials containing muscle artifacts were rejected from further
1276 analysis using a standard semi-automatic preprocessing method in Fieldtrip. This
1277 procedure consists of bandpass-filtering the trials of a condition block in the 110–125
1278 Hz frequency range, which typically contains most of the muscle artifact activity,
1279 followed by a Z-transformation. Trials exceeding a threshold Z-score were removed
1280 completely from analysis. We used as the threshold the absolute value of the
1281 minimum Z-score within the block, + 1. To remove eye blink artifacts from the time
1282 courses, the EEG data from a complete session were transformed using
1283 independent component analysis (ICA), and components due to blinks (typically one
1284 or two) were removed from the data. In addition, to remove microsaccade-related
1285 artifacts we included two virtual channels in the ICA based on channels Fp1 and
1286 Fp2, which included transient spike potentials as identified using the saccadic

1287 artefact detection algorithm from Hassler et al. (2011). This yielded a total number of
1288 channels submitted to ICA of $48 + 2 = 50$. The two components loading high on
1289 these virtual electrodes (typically with a frontal topography) were also removed.
1290 Blinks and eye movements were then semi-automatically detected from the
1291 horizontal and vertical EOG (frequency range 1–15 Hz; z-value cut-off 4 for vertical;
1292 6 for horizontal) and trials containing eye artefacts within 0.1 s around target onset
1293 were discarded. This step was done to remove trials in which the target was not
1294 seen because the eyes were closed. Finally, trials exceeding a threshold voltage
1295 range of $200 \mu\text{V}$ were discarded. To attenuate volume conduction effects and
1296 suppress any remaining microsaccade-related activity, the scalp current density
1297 (SCD) was computed using the second-order derivative (the surface Laplacian) of
1298 the EEG potential distribution (Perrin et al., 1989).

1299 **ERP analysis** We computed event-related potentials in electrode C4 by low-pass
1300 filtering the time-domain data up to 8 Hz followed by averaging all trials within
1301 participant per condition.

1302 **Spectral analysis** We used a sliding window Fourier transform (Mitra & Pesaran,
1303 1999); step size, 50 ms; window size, 400 ms; frequency resolution, 2.5 Hz) to
1304 calculate time-frequency representations (spectrograms) of the EEG power for each
1305 electrode and each trial. We used a single Hann taper for the frequency range of 3–
1306 35 Hz (spectral smoothing, 4.5 Hz, bin size, 1 Hz) and the multitaper technique for
1307 the 36 – 100 Hz frequency range (spectral smoothing, 8 Hz; bin size, 2 Hz; five
1308 tapers). See Kloosterman et al. (2015) and Meindertsma et al. (2017) for similar
1309 settings. Finally, to investigate spectral power also < 3 Hz, we ran an additional time-
1310 frequency analysis with a window size of 1 s (i.e. frequency resolution 1 Hz)

1311 centered on the time point 0.5 s before trial onset (frequency range 1–35 Hz, no
1312 spectral smoothing, bin size 0.5 Hz).

1313 Spectrograms were aligned to the onset of the stimulus sequence containing
1314 the (non)target. Power modulations during the trials were quantified as the
1315 percentage of power change at a given time point and frequency bin, relative to a
1316 baseline power value for each frequency bin (Figure 3). We used as a baseline the
1317 mean EEG power in the interval 0.4 to 0 s before trial onset, computed separately for
1318 each condition. If this interval was not completely present in the trial due to
1319 preceding events (see Trial extraction), this period was shortened accordingly. We
1320 normalized the data by subtracting the baseline from each time-frequency bin and
1321 dividing this difference by the baseline (x 100 %). For the analysis of raw pre-
1322 stimulus power modulations, no baseline correction was applied on the raw scalp
1323 current density values. We focused our analysis of EEG power modulations around
1324 target onsets on those electrodes that processed the visual stimulus. To this end, we
1325 averaged the power modulations or raw power across eleven occipito-parietal
1326 electrodes that showed stimulus-induced responses in the gamma-band range (59–
1327 100 Hz). See Kloosterman et al. (2015) and Meindertsma et al. (2017) for a similar
1328 procedure.

1329 **Statistical significance testing of EEG power modulations across space, time**
1330 **and frequency.** To determine clusters of significant modulation with respect to the
1331 pre-stimulus baseline without any a priori selection, we ran statistics across space-
1332 time-frequency bins using paired t-tests across subjects performed at each bin.
1333 Single bins were subsequently thresholded at $p < 0.05$ and clusters of contiguous
1334 time-space-frequency bins were determined. Cluster significance was assessed
1335 using a cluster-based permutation procedure (1000 permutations). For visualization

1336 purposes, we integrated (using the matlab trapz function) power modulation in the
1337 time-frequency representations (TFR's, left panels) across the highlighted electrodes
1338 in the topographies (right panels). For the topographical scalp maps, modulation was
1339 integrated across the saturated time-frequency bins in the TFRs. To test at which
1340 frequencies raw prestimulus EEG power differed between the liberal and
1341 conservative conditions, we performed this analysis across electrodes and space
1342 after taking the liberal – conservative difference at each frequency bin (Figure 4C)
1343 (see Statistical comparisons).

1344 **Response gain model test** To test the predictions of the gain model, we first
1345 averaged activity in the 8–12 Hz range from 0.8 to 0.2 s before trial onset (staying
1346 half our window size from trial onset, to avoid mixing pre- and poststimulus activity,
1347 also see Iemi et al. (2017)), yielding a single scalar alpha power value per trial. If this
1348 interval was not completely present in the trial due to preceding events (see Trial
1349 extraction), this period was shortened accordingly. Trials in which the scalar was > 3
1350 standard deviations away from the participant's mean were excluded. We then
1351 sorted all single-trial alpha values for each participant and condition in ascending
1352 order and assigned them to ten bins of equal size, ranging from weakest to strongest
1353 alpha. Adjacent bin ranges overlapped for 50% to stabilize estimates. Then we
1354 averaged the corresponding gamma modulation of the trials belonging to each bin
1355 (consisting of the average power modulation within 59–100 Hz 0.2 to 0.6 s after trial
1356 onset, see Figure 3). Finally, we averaged across participants and plotted the
1357 median alpha value per bin averaged across participants against gamma
1358 modulation. See Rajagovindan and Ding (2011) for a similar procedure. To
1359 statistically test for the existence of inverted U-shaped relationships between alpha
1360 and gamma, we performed a one-way repeated measures ANOVA on gamma

1361 modulation with factor alpha bin (10 bins) to each condition separately and a two-
1362 way repeated measures ANOVA with factors bin and condition for testing the liberal–
1363 conservative difference (Figure 5F). Given the model prediction of a Gaussian-
1364 shaped relationship between alpha and gamma, we constructed a Gaussian contrast
1365 using the normal Gaussian shape with unit standard deviation (contrast values: -
1366 1000, -991, -825, 295, 2521, 2521, 295, -825, -991, -1000, values were chosen to
1367 sum to zero). For plotting purposes (Figure 5C-F), we computed within-subject error
1368 bars by removing within each participant the mean across conditions from the
1369 estimates.

1370 **Correlation between gamma modulation and drift bias** To link DDM drift bias and
1371 cortical gamma power, we re-fitted the DDM drift bias model while freeing the drift
1372 bias parameter both for each condition as well as for the ten alpha bins, while freeing
1373 the other parameters (drift rate, boundary separation, non-decision time) for each
1374 condition and fixing starting point across conditions. We then used repeated
1375 measures correlation to test whether stronger gamma was associated with stronger
1376 bias. Repeated measures correlation determines the common within-individual
1377 association for paired measures assessed on two or more occasions for multiple
1378 individuals by controlling for the specific range in which individuals' measurements
1379 operate, and correcting the correlation degrees of freedom for non-independence of
1380 repeated measurements obtained from each individual. Specifically, the correlation
1381 degrees of freedom were $14 \text{ participants} \times 10 \text{ observations} - \text{Number of participants}$
1382 $- 1 = 140 - 14 - 1 = 125$. Repeated measures correlation tends to have much
1383 greater statistical power than conventional correlation across individuals because
1384 neither averaging nor aggregation is necessary for an intra-individual research
1385 question. Please see Bakdash and Marusich (2017) for more information. We

1386 assessed the impact of single observations on the correlations by excluding
1387 observations exceeding five times the average Cook's distance of all values within
1388 each condition (five observations for liberal and four for conservative) and
1389 recomputing the correlations.

1390 **Statistical comparisons** We used two-sided permutation tests (10,000
1391 permutations) (Efron & Tibshirani, 1998) to test the significance of behavioral effects
1392 and the model fits. Permutation tests yield $p = 0$ if the observed value falls outside
1393 the range of the null distribution. In these cases, $p < 0.0001$ is reported in the
1394 manuscript. The standard deviation (s.d.) is reported as a measure of spread along
1395 with all participant-averaged results reported in the text. To quantify power
1396 modulations after (non-)target onset, we tested the overall power modulation for
1397 significant deviations from zero. For these tests, we used a cluster-based
1398 permutation procedure to correct for multiple comparisons (Maris & Oostenveld,
1399 2007). For time-frequency representations along with spatial topographies of power
1400 modulation, this procedure was performed across all time-frequency bins and
1401 electrodes; for frequency spectra across all electrodes and frequencies; for power
1402 and ERP time courses, across all time bins. To test the existence of inverted-U
1403 shaped relationships between gamma and alpha bins, we conducted repeated
1404 measures ANOVA's and Gaussian shaped contrasts (see section Response gain
1405 model test for details) using SPSS 23 (IBM, Inc.). We used multiple regression to
1406 assess whether starting point could account for the correlation between gamma and
1407 drift bias. We used Pearson correlation to test the link between parameter estimates
1408 of the DDM and SDT frameworks and repeated measures correlation to test the link
1409 between gamma power and drift bias (see previous section).